AEDC-TDR-63-130

Cy 2

INVESTIGATION OF TWO-NOZZLE CLUSTER DIFFUSER-EJECTOR WITH AND WITHOUT EJECTED MASS

By

James W. Hale

Rocket Test Facility

ARO, Inc.

TECHNICAL DOCUMENTARY REPORT NO. AEDC-TDR-63-130

November 1963

AFSC Program Area 921E

(Prepared under Contract No. AF 40(600)-1000 by ARO, Inc., contract operator of AEDC, Arnold Air Force Station, Tenn.)

ARNOLD ENGINEERING DEVELOPMENT CENTER

AIR FORCE SYSTEMS COMMAND

UNITED STATES AIR FORCE

NOTICES

Qualified requesters may obtain copies of this report from DDC, Cameron Station, Alexandria, Va. Orders will be expedited if placed through the librarian or other staff member designated to request and receive documents from DDC.

When Government drawings, specifications or other data are used for any purpose other than in connection with a definitely related Government procurement operation, the United States Government thereby incurs no responsibility nor any obligation whatsoever; and the fact that the Government may have formulated, furnished, or in any way supplied the said drawings, specifications, or other data, is not to be regarded by implication or otherwise as in any manner licensing the holder or any other person or corporation, or conveying any rights or permission to manufacture, use, or sell any patented invention that may in any way be related thereto.

AEDC-TDR-63-130

INVESTIGATION OF TWO-NOZZLE CLUSTER DIFFUSER-EJECTOR WITH AND WITHOUT EJECTED MASS

By

James W. Hale

Rocket Test Facility

ARO, Inc.

a subsidiary of Sverdrup and Parcel, Inc.

November 1963

ARO Project No. RM1146

AF - AEDC
Arnold AFS Tenn

ABSTRACT

An investigation was conducted to determine the best shape for a diffuser-ejector configuration for a two-nozzle cluster rocket and included the performance of various combinations of configurations derived from six basic diffuser-ejector geometric shapes and sizes and four basic arrangements of nozzle configurations. The performance was obtained for all configurations both with and without ejected mass from the test cell. The ejected mass from the test cell was accomplished by two parallel auxiliary jet pumps. The simulated rocket nozzles were conical 13.25-deg half angle. Unheated dry air was used as the driving fluid for the simulated rocket and jet pumps. Saturated 200-psig steam was also used as a jet pump driving fluid.

The obround diffuser performed better than the circular diffuser of equal cross-sectional area for the two-nozzle cluster configuration. The starting and operating pressure ratios for the straight diffuser configurations varied with diffuser length-to-diameter ratio. The maximum of 90 percent of the one-dimensional normal shock total pressure ratio was determined for a diffuser length-to-diameter ratio of 8. The starting and operating pressure ratio for the second throat configuration was equal to or greater than the one-dimensional normal shock pressure ratio for a second throat length-to-diameter ratio between 4 and 5. Little change in diffuser-ejector performance resulted from dividing the ducts by a partition except for a second-throat configuration which did not start when the partition was extended through the contracted section. For the second-throat configuration, the starting and operating pressure ratio increased when the second-throat contraction decreased. For the two configurations tested, the presence of a second throat with a contraction ratio of approximately 0.60 produced an improvement of approximately 15 percent in the cell-to-chamber pressure ratio. The small duct-to-nozzle throat area ratio configurations gave isentropic and better cell-to-chamber pressure ratios, whereas the large duct-to-nozzle throat area ratio configurations gave greater than isentropic cell-to-chamber pressure ratios (as high as 1.62 times the one-dimensional isentropic value). An improvement by a factor of 10

ILLUSTRATIONS

NOMENCLATURE

A_d	Cross-sectional area of diffuser duct, $in.^2$
A_{ne}	Cross-sectional area of nozzle exit, $in.^2$
A_{st}	Cross-sectional area of second throat duct, $in.^2$
A^*	Cross-sectional area of nozzle throat, $in.^2$
B	Overall length of second-throat diffuser
D	Diameter of diffuser duct, in.
d	Diameter of diffuser second-throat duct, in.
L	Length of diffuser duct at diameter, D, in.
ℓ	Length of diffuser second-throat duct, in.
M_d	Diffuser duct Mach number
P_c	Simulated rocket cell pressure, psia
P_{c1}	Jet pump number 1 cell or secondary pressure, psia
P_{c2}	Jet pump number 2 cell or secondary pressure, psia
P_t	Simulated rocket chamber total pressure, psia
P_{t1}	Jet pump number 1 driving or primary pressure, psia
P_{t2}	Jet pump number 2 driving or primary pressure, psia
P_{ex}	Diffuser duct exit pressure, psia
R	Radius from centerline of simulated rocket nozzle centerline at distance x from the simulated rocket nozzle exit, in.
T_{t1}	Jet pump number 1 driving fluid total temperature, °F
T_{t2}	Jet pump number 2 driving fluid total temperature, °F
T_t	Simulated rocket driving fluid total temperature, °F
W_a	Simulated rocket mass weight flow, lb_m/sec
W_b	Jet pumps total ejected or secondary mass weight flow, lb_m/sec
W_p	Jet pumps total driving fluid or primary mass weight flow, lb_m/sec
X	Distance from the nozzle exit to the beginning of the second throat, in.

x	Distance measured from simulated rocket nozzle exit plane, in.
z	Distance from nozzle exit to diffuser inlet (Minus sign indicates that the diffuser inlet is upstream of the nozzle exit, and plus sign indicates that the diffuser inlet is downstream of the nozzle exit.)

SUBSCRIPTS

act	Actual
st	Second throat
ns	Normal shock
isen	Isentropic
pred	Predicated

SUPERSCRIPTS

1	Ejected mass from the simulated rocket test cell

1.0 INTRODUCTION

Results of the cold-flow, two-nozzle-cluster model study conducted in the Rocket Test Facility (RTF), Arnold Engineering Development Center (AEDC), Air Force Systems Command (AFSC), from December 4, 1961, to April 4, 1962, are presented. The investigation was performed to determine the diffuser-ejector configuration which would best satisfy engine test requirement. The requirement of the full-scale test program and space limitation in the J-3 altitude test cell impose severe restrictions on the shape and size of the diffuser that can be used.

Much work has been reported on single nozzles in single circular duct configurations without induced mass into the test cell. Little or no literature is available giving performance of nozzle clusters in various-shape ducts and with ejected mass from the test cell.

Six basic series of diffuser-ejector geometric configurations were selected. Various combinations of nozzle configurations were used to drive the diffuser configurations being tested. The performance of the various diffuser-ejector configurations was obtained both with and without ejected mass from the test cell.

The major consideration of the investigation was the effect of the diffuser geometric shape on ejector performance and the effect of ejected mass from the test cell on the ejector performance. Correlation of model data and one-dimensional isentropic relationship between diffuser-to-nozzle throat area ratio, $\Sigma(A_d/A^*)$, cell-to-nozzle total pressure ratio, P_c/P_t, and ratio of specific heats, γ, is shown.

2.0 APPARATUS

The six basic series tested were composed of either one axisymmetric simulated rocket nozzle concentrically or eccentrically located or two axisymmetric simulated rocket nozzles eccentrically located 180 deg apart.

2.1 SIMULATED ROCKET NOZZLE PLENUM SECTION

A 4-in. schedule 160 pipe 15-3/8 in. long welded to a 12-in. flange was used as the simulated rocket nozzle plenum chamber. The simulated

---

Manuscript received May 1963.

rocket nozzles were installed on the plenum chamber by means of an adapter head. One of two adapter heads was used, depending on the simulated rocket nozzle configuration being tested. The different nozzle configurations are presented in Fig. 1. The nozzle plenum section was located in a sealed plenum or test cell section to which the diffusers were attached. A typical test configuration is shown in Fig. 2.

The simulated rocket nozzles were different only in throat diameters which were 0.51 in. for -2 nozzle and 0.50 in. for -3 nozzle. The axisymmetric 13.25-deg, half-angle conical nozzle had an exit-to-throat area ratio of $A_{ne}/A^* = 12.25$. Dimensional details of these nozzles are presented in Fig. 3.

2.2 SIMULATED ROCKET NOZZLE TEST CELL

The test cell consists of a duct 12 in. in diameter and 21.00 in. long, to which two parallel air or steam driven auxiliary jet pumps are perpendicularly attached 180 deg apart. The jet pumps discharge to the facility exhaust ducting downstream of the hand operated isolation valve. Two 4-in. gate valves separate the test cell from the jet pumps.

The jet pumps consist of an axisymmetric 9-deg, half-angle conical nozzle installed on a plenum chamber section consisting of a 1-1/2 in. schedule double, extra-heavy pipe approximately 13 in. long and installed inside the 4-in. standard schedule 40 ducts as shown in Fig. 2. The nozzles for both pumps are identical with throat diameters of 0.437 in. The exit to throat nozzle area ratio of the jet pump nozzles is $A_{ne}/A^* = 25.12$. Details of these nozzles are presented in Fig. 4.

2.3 DUCT AND NOZZLE DESIGNATION

Included in the Summary of Test Data (Table 1) are the duct and nozzle configuration code designations of the nozzle and diffuser combinations. This duct and nozzle configuration code designation combines the nozzle configuration code (Fig. 1) and the diffuser configuration code (Fig. 5). A typical duct and nozzle configuration designation as listed in Table 1 is 1a-A (diffuser configuration 1a from Fig. 5a, and nozzle configuration A from Fig. 1). The S preceding the diffuser configuration code as in Fig. 5c designates the second-throat diffuser for that configuration.

2.4 DIFFUSER INSTALLATION

A 24-in. space shown in Fig. 2 existed between the downstream face of the test cell and the upstream face of the transition section to the

exhaust ducting for installation of the various diffuser configurations. Part of the six basic diffuser configurations presented in Fig. 5 (1, 2, S2, 4, and 5) were flange connected to the test cell downstream flange and the upstream flange of the transition section (Fig. 2). The remaining configurations (3, S3, S4, S5, and S6) were installed inside a circular duct which was flange connected between the test cell and the transition section.

2.4.1 Variable Axial Position Diffuser

The axial position of the duct mounted diffuser configurations was made variable by a connection to a gear train mechanism located inside the test cell on the test cell downstream flange. During the test the mechanism was operated by a hand wheel outside the test cell.

2.4.2 Diffuser Configuration 1 Series

Various cross-sectional shapes and sizes of straight and second-throat diffuser configurations were investigated. The single duct, circular, cross-sectional diffuser designated as configuration 1 is presented in detail in Fig. 5a. Three of these circular configurations with diameters of 5.288, 6.065, and 4.680 in. were designated as duct configurations 1a, 1b, and 1c, respectively. The fourth configuration, designated as 1d, was the same as 1c except a 1.50-in. extension was added to the inlet end of the 1c configuration so that the nozzle exit plane would be in the plane of the diffuser inlet. Only the nozzle configuration A was used to drive the series 1 configurations.

2.4.3 Diffuser Configuration 2 Series

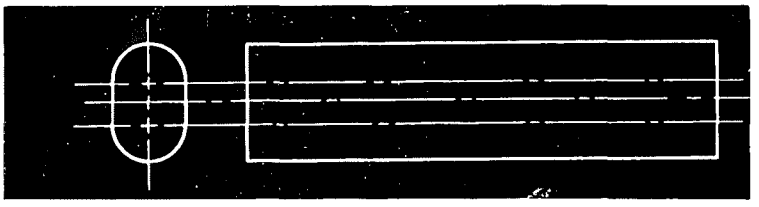

The diffuser configuration 2 series consisted of an obround cross-sectional shape with the distance between the centerlines of the circular sections equal to the distance between the two nozzles. The obround diffuser was a more symmetrical diffuser configuration for a two-nozzle cluster than was a single circular diffuser. The details of the obround diffuser are presented in Fig. 5b. Three variations of this configuration 2 series were made by installing a short 1/16-in. -thick

partition and a full length 1/16-in.-thick partition. Duct configuration 2a had no partition, 2b had a short partition, and 2c had a full length partition.

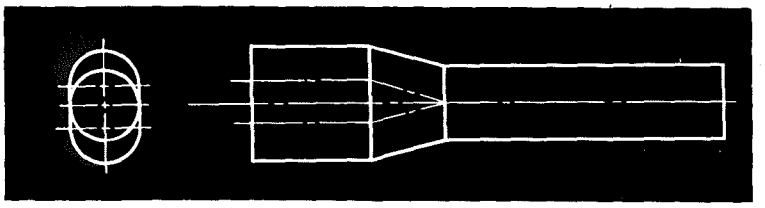

The obround diffuser (configuration 2) was equipped with a circular second-throat and designated S2; configuration details are presented in Fig. 5c. Three variations in the S2 configuration, which had a contraction area ratio, A_{st}/A_d of 0.5744, were tested. Configurations S2a and S2c were constructed similarly to configurations 2a and 2c, respectively, whereas configuration S2b had a partition that extended through the transition to the second throat. The configurations 2 and S2 series were driven by only the nozzle configuration A.

2.4.4 Diffuser Configuration 3 Series

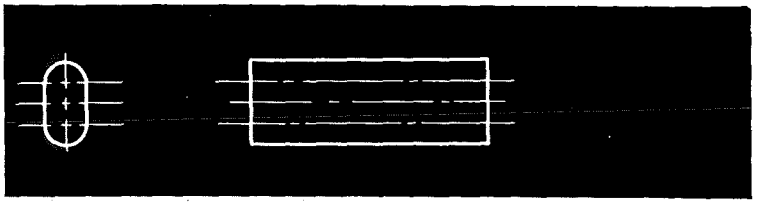

A smaller series of obround diffusers having both constant cross-sectional flow area and a second-throat was tested. The spacing between the centerlines of the circular sections was the same as the 2 series (2.19 in.). Only the radius of the circular sections was smaller. The details of configuration 3 are presented in Fig. 5d.

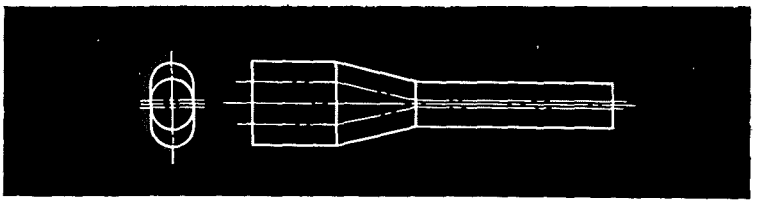

Diffuser configuration S3 consisted of an obround diffuser and second-throat. Two lengths of capture duct were tested. Nozzle configurations A, B, and C were employed.

2.4.5 Diffuser Configuration 4 Series

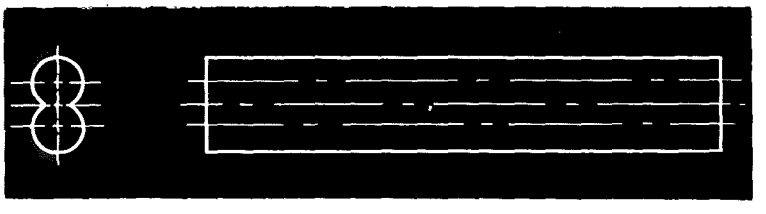

The fourth series of diffuser configurations tested was a straight twin intersecting circular diffuser as shown in Fig. 5f. The centerline of the two intersecting circular ducts coincided with the centerline of the nozzles in configuration A. The configuration 4 was tested

both without a partition between the intersecting ducts (4a) and with a 1/16-in. -thick partition (4b).

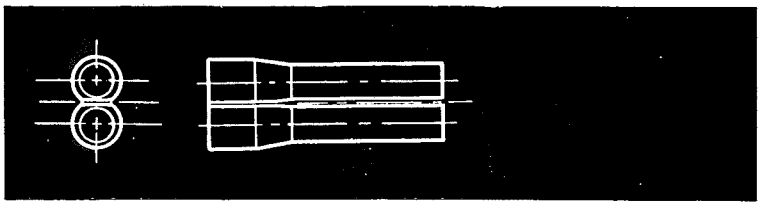

A twin second-throat configuration with an identical inlet to the diffuser configuration 4 was tested with nozzle configurations A, B, and C. Two contraction area ratios were investigated. The smaller second-throat contraction (second-throat diameter of 1.854 in.) was designated as S4a, while the larger second-throat contraction (second-throat diameter of 1.936 in.) was designated as S4b. The details of the S4 configuration are presented in Fig. 5g.

2.4.6 Diffuser Configuration 5 Series

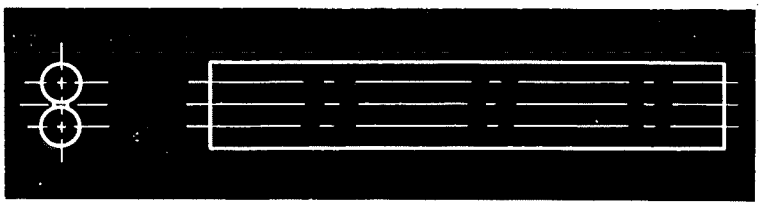

The fifth series of configurations consisted of a straight twin circular diffuser, designated as configuration 5. The only difference between diffuser configuration 5 and diffuser configuration 4 (Fig. 5f) was the duct diameter. Configuration 5 was made with ducts sufficiently small that they did not intersect when spaced so that the centerlines of the duct and nozzles of configuration A coincided (2.19 in.). These details are presented in Fig. 5h.

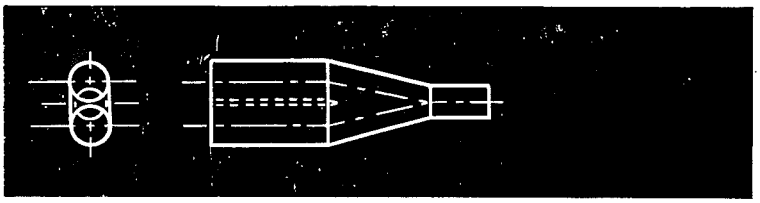

The second-throat configuration for configuration 5 consisted of a single duct circular cross section. The second-throat configuration was designated as S5 with details presented in Fig. 5i. Six different contraction area ratios with an inlet section length of 6.0 in. were investigated. The configurations were designated as S5a, S5b, S5c, S5d, S5e, and S5f for increasing contraction area ratio as shown in the table in Fig. 5i. The only difference in S5f and S5g was that the 6.0-in. inlet length L for S5f was reduced to 2.065 in.

2.4.7 Diffuser Configuration 6 Series

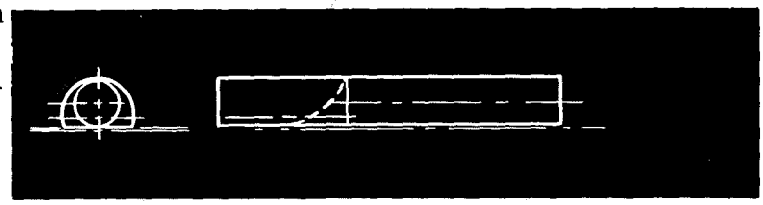

A single duct section of a second-throat twin intersecting circular diffuser with inlet cross section completely nonsymmetrical with the nozzle and a circular second throat with centerline offset from the centerline of the nozzle was tested with nozzle configuration C driving the diffuser. The details of this diffuser configuration designated as S6 are presented in Fig. 5j. The S6 diffuser cross section approaches an obround shape, but the centerline of the circular section was offset from the centerline of the nozzle, while for the obround configurations the centerlines coincided. The second-throat contraction area ratio for S6 diffuser configuration was $A_{st}/A_d = 0.5732$.

2.5 SIMULATED ROCKET NOZZLE AND JET PUMP DRIVING FLUID

Air from the VKF 4000-psi storage tank or 200 psig saturated steam from the AEDC central plant provided the driving media for the auxiliary jet pumps which discharged to the RTF facility exhaust machines. The same air from the VKF 4000-psi storage tank provided the driving medium for the simulated rocket nozzles with a plenum total pressure that ranged from 254 to 450 psia. The diffuser-ejectors exhausted to the RTF facility exhaust machines which maintained a pressure as low as 0.12 psia. The 20-in., hand-operated gate valve (Fig. 2) was used to vary the exhaust pressure at the exit of the diffuser-ejector.

2.6 INSTRUMENTATION

The parameters of primary interest were cell pressures for the two jet pumps and the diffuser-ejector P_{c1}, P_{c2}, and P_c; diffuser exit pressure, P_{ex}; jet pump and simulated rocket nozzle plenum total pressure, P_{t1}, P_{t2}, and P_t; and plenum total temperature for the jet pumps and the simulated rocket nozzle, T_{t1}, T_{t2}, and T_t.

All pressures were read on diaphragm activated dial gages. These gages were periodically calibrated and the readings were well within the calibration range. The temperatures were measured with copper-constantan thermocouples and read on compensating millivolt meters. All parameters were recorded manually after a steady-state condition was reached.

2.7 JET PUMP CALIBRATION

A calibration of the jet pumps was accomplished by installing a flange of five venturis on the inlet to the jet pump cell valve which connects the jet pump to the test cell (Fig. 2). The five venturis were used to measure accurately the atmospheric inbleed or secondary airflow into the jet pump cell region. The secondary airflow was varied by inbleeding through one or more of the five venturis. Rubber plugs were used to isolate the venturis for varying the secondary airflow.

The jet pump cell or secondary pressure was measured for the various atmospheric inbleed airflows for a range of jet pump driving pressures with both air and steam as the jet pump driving medium. The jet pump calibration was used to determine accurately the ejected mass of air from the test cell of the diffuser-ejector configuration being tested.

3.0 TEST PROCEDURE

At the beginning of each test a vacuum check was made to detect any possible leaks into the system before any data were taken.

The test objective was to measure the performance of each test configuration as a diffuser-ejector by finding the minimum cell-to-nozzle total pressure ratio, P_c/P_t, and the corresponding starting and operating pressure ratios, P_{ex}/P_t, in order to determine the best configuration for the two nozzle cluster. A typical ejector performance curve defining the starting and operating pressure ratios is presented in Fig. 3 of Ref. 1.

The data were obtained by setting the desired nozzle plenum total pressure with the exhaust pressure set low enough to ensure ejector starting and then increasing the exhaust pressure until the ejector became unstarted. This point determined the operating pressure ratio. The exhaust pressure was then decreased until the ejector became started. This point determined the starting pressure ratio. The procedure was repeated for various simulated rocket nozzle plenum total pressure levels.

3.1 SECOND-THROAT POSITIONING

The variable axial position second-throat configurations were tested at various positions to determine the maximum distance from the nozzle exit to the beginning of the second throat for the diffuser-ejector to start,

operate at minimum pressure ratio, P_c/P_t, and restart. The axial position of the diffuser was varied until breakdown and then repositioned until it restarted again. In some cases, the diffuser was positioned before the airflow through the nozzles was started. If the diffuser-ejector did not start, the airflow was stopped and the diffuser was repositioned. This was continued until the diffuser started or until the limit of positioning was reached.

3.2 IMPROVED PERFORMANCE BY JET PUMPS

All configurations were tested to determine the decrease in minimum pressure ratio, P_c/P_t, by ejecting mass from the test cell with the jet pumps. While the diffuser was started and operating at its minimum pressure ratio, P_c/P_t, and while the jet pumps were operating at no secondary flow, one or both of the 4-in. hand valves between the diffuser-ejector test cell and the jet pump cell region was either opened in steps from closed to fully open or all the way open in one step. By opening the valves in steps while data were recorded, the decrease in P_c/P_t with an increase in ejected mass flow to simulated rocket mass flow, W_b/W_a, was determined. The maximum decrease in P_c/P_t occurred when both jet pumps were pumping at maximum efficiency with valves opened to the test cell. The start and operate driving pressure ratio, P_{ex}/P_t, was determined with the jet pumps ejecting mass from the test cell for comparison with the no ejected mass condition.

4.0 RESULTS AND DISCUSSION

A summary of the data from the configurations tested and the experimental results compared with one-dimensional isentropic values from Ref. 2 is presented in Table 1 and in Figs. 6 through 22.

4.1 STRAIGHT DIFFUSERS DRIVEN BY TWO-NOZZLE CLUSTER

The basic straight diffuser configurations tested with two simulated rocket nozzles were circular, twin intersecting circular, twin circular, and obround cross-sectional ducts. Sketches of these configurations are presented in Figs. 5a, b, d, f, and h.

The performance for configurations 1c-A and 1d-A is presented in Fig. 6. Configuration 1d-A has the lower P_c/P_t ratio and the higher P_{ex}/P_t ratio. This difference can be explained by looking at the simulated

rocket nozzle free-jet boundary. The free-jet boundary, which was calculated by the method presented in Ref. 3, is shown as a typical jet boundary in Fig. 7. When the diffuser configuration 1c-A is drawn in Fig. 7 with the inlet of the diffuser 1.50 in. downstream of the nozzle exit, the jet boundary intersects the diffuser near its inlet. The free-jet boundary is shown as a line in Fig. 7, but actually the boundary has thickness referred to as the mixing zone. The thickness of the boundary increases with distance downstream of the nozzle exit as presented in Refs. 4 and 5. Since the free-jet boundary is near the inlet of the diffuser at the nearest point to the nozzle centerline, low energy air (outer portion of the mixing zone) is spilled into the cell which results in an increase in cell pressure. This spillage causes a decrease in start and operate driving pressure ratio, P_{ex}/P_t, and an increase in the ratio, P_c/P_t, as shown in Fig. 6.

Since the inlet of the diffuser of configuration 1d-A is in the same plane as the nozzle exit and since the jet boundary intersects the diffuser downstream of the diffuser inlet, no spillage of the low-energy, high-pressure air into the test cell is evident.

The free-jet boundary for configuration 1a-A intersects near the diffuser inlet over a small region at the nearest point on the duct from the nozzle centerline. Spillage of low-energy high-pressure air into the test cell occurred over this small region. Since the inlet of this diffuser was not moved closer to the nozzle exit, it is not known what minimum ratio, P_c/P_t, could have been obtained by this 5.288-in.-diam diffuser.

The free-jet boundary impingement on configuration 1b-A is downstream of the diffuser inlet. There is no evidence of spillage of the low-energy boundary air into the cell for this 6.065-in.-diam diffuser configuration.

The performance of all the straight diffusers tested is presented in Fig. 8. An ejector rise ratio, $P_{ex}/P_c = 26$ is shown for configurations 1a-A and 1b-A. A value of 21.5 is shown for 1d-A.

The driving pressure ratio, P_{ex}/P_t, required to start the ejectors decreased as the duct-to-nozzle throat area ratio, $\Sigma(A_d/A^*)$, increased. The larger ducts required a smaller exit pressure for the ejector to start and operate than did the smaller ducts. This starting and operating behavior is the same as was found with single nozzles in circular ducts presented in Fig. 8 of Ref. 6.

The minimum P_c/P_t pumped decreased with an increase in $\Sigma(A_d/A^*)$. This agrees with the trend for a single nozzle in single ducts as presented in Fig. 9 of Ref. 6.

The twin intersecting circular duct and nozzle configuration 4a-A (Fig. 5f) had an ejector rise ratio, P_{ex}/P_c = 26.5 and a driving pressure ratio, P_{ex}/P_t = 0.0556 (Fig. 8). The rise ratio of 26.5 is very close to the rise ratio of 26 obtained for the two larger circular ducts, configurations 1a-A and 1b-A, but the driving pressure ratios differ considerably. The 4a-A configuration had a $\Sigma(A_d/A^*)$ = 23.36 and an L/D = 10.68.

The twin circular duct configuration 5-A (Fig. 5h) was similar to the twin intersecting circular duct, 4a-A (Fig. 5f). Figure 8 shows an ejector rise ratio, P_{ex}/P_c = 21, and a driving pressure ratio, P_{ex}/P_t = 0.0723, for 5-A. The 5-A configuration had a $\Sigma(A_d/A^*)$ = 16.72 and an L/D = 12.77.

The two obround ducts tested, configurations 2a-A and 3-A (Figs. 5b and d), had a $\Sigma(A_d/A^*)$ = 42.97 and 19.65, respectively. The L/D for the two configurations were 6.76 and 5.81. The minor diameters were used to calculate the L/D ratios. As shown in Fig. 8, the rise ratios are 22 for the small duct 3-A and 29 for the large duct 2a-A.

The larger of the obround ducts, configuration 2a-A, had the same cross-sectional area as the 4.680-in.-diam circular duct, configuration 1d-A, but the rise ratio for 2a-A was much higher (29 as compared with 21.5 in Fig. 8). The maximum P_c/P_t for the obround duct was about 76 percent of the P_c/P_t for the circular duct. This P_c/P_t improvement of 24 percent obtained from the obround duct over the circular duct was a result of having a more symmetrical duct and nozzle configuration.

Figure 9 is a plot of P_{ex}/P_t vs $\Sigma(A_d/A^*)$ for the seven configurations just discussed and the theoretical one-dimensional normal shock total pressure ratio (P_{ty}/P_{tx} where x is upstream of normal shock and y is downstream) obtained from Ref. 2. The line through the actual data points parallels the theoretical normal shock line. This indicates that a constant exists between the theoretical normal shock total pressure ratio and the experimental driving pressure ratio, P_{ex}/P_t, for the seven configurations. The average ratio of $P_{ex}/P_t \,/\, P_{ty}/P_{tx}$ for the seven configuration is 0.7993 and is represented by the solid line through the data points in Fig. 9. The points for configurations 1a-A and 1c-A were not considered because the spillage of the high-pressure, low-energy air from the free-jet boundary into the test cell resulted in a lower P_{ex}/P_t than would have been obtained if there had been no spillage. The lower P_{ex}/P_t results are presented in Fig. 6 for configurations 1c-A and 1d-A. A straight line can be drawn through the points for 1b-A, 1a-A, and 1c-A. The rate of decrease in P_{ex}/P_t from the 0.7993 data

line (Fig. 9) increased as the diameter of the diffuser decreased. As the diameter decreased, the spillage increased. Figure 6b of Ref. 7 presents the single nozzle in single duct driving pressure ratio, P_{ex}/P_t, deviation from theoretical normal shock total pressure ratio. This deviation was 90 percent for conical nozzles in circular ducts with L/D = 8 without a subsonic diffuser.

The difference in the L/D ratios for the seven configuration and the fact that some of the experimental points fall above and below the average line (Fig. 9) indicate that an optimum L/D ratio exists. When the ratio $P_{ex}/P_t \,/\, P_{ty}/P_{tx}$ is plotted as a function of L/D for the above configuration, the optimum L/D can be determined. Figure 10 presents such a plot. The optimum L/D of 8 corresponds to a maximum ratio of $P_{ex}/P_t \,/\, P_{ty}/P_{tx} = 0.90$. The large obround duct configuration 2a-A had an L/D of 6.76 which is close to the optimum of 8 and agrees with that obtained in Ref. 7 for a single nozzle in a single duct without subsonic diffuser.

The respective rise ratio, P_{ex}/P_c, increase of 21.5 to 29, or 34.9 percent increase, for the circular configuration 1d-A and obround configuration 2a-A was a result of having an effective L/D increase toward optimum. The small obround duct 3-A and the circular duct 1d-A have equal rise ratios and approximately equal L/D's, 5.81 and 5.45. The difference in L/D for the seven configurations presented in Fig. 10 accounts for the different rise ratios.

4.2 STRAIGHT OBROUND DIFFUSERS

The performance of configurations 2a-A, 2b-A, and 2c-A is presented in Fig. 11a. The partitions in the 2b and 2c diffusers caused an increase in P_c/P_t from 0.001040 to 0.001211. This increase in P_c/P_t was caused partially by the reduction in $\Sigma(A_d/A^*)$, partially by the nonsymmetry of the duct and nozzle, partially by the friction (area of wetted surface increase), and partially by shock losses. This is indicated by the difference in the ratios

$$\frac{(P_c/P_t)_{\text{without partition}}}{(P_c/P_t)_{\text{with partition}}} = 0.86 \text{ and } \frac{(P_c/P_t)_{\text{isen without partition}}}{(P_c/P_t)_{\text{isen with partition}}} = 0.98.$$

If these ratios were equal, then the reduction in $\Sigma(A_d/A^*)$ could have been totally responsible for the increase in P_c/P_t.

There was essentially no difference in the start and operate driving pressure ratio, $P_{ex}/P_t = 0.031$. The partitioned ducts had a rise ratio, $P_{ex}/P_c = 25$, while the duct without a partition had a rise ratio of 29.

4.3 OBROUND SECOND-THROAT DIFFUSERS

The performance of the three configurations (S2a-A, S2b-A, and S2c-A) is presented in Fig. 11b. The obround inlet of diffuser configuration S2a had the same cross-sectional area as did diffuser 2a except for fabrication tolerance. Configuration S2a-A had a ratio $P_c/P_t = 0.00110$, which was a little higher than the ratio $P_c/P_t = 0.00104$ for 2a-A. When the short partition was installed (S2b-A), the P_c/P_t increased from 0.00110 to 0.00119 (Fig. 11b). The $P_c/P_t = 0.00119$ for S2b-A is in good agreement with the $P_c/P_t = 0.00121$ (Fig. 11b) for 2b-A. The minimum ratio, P_c/P_t, for S2c-A which had the partition extending through the second throat was 0.00320. The $P_c/P_t = 0.00320$ pumped by S2c-A corresponds to a theoretical area ratio $A_d/A^* = 17.42$ from Ref. 2 which was between the actual $\Sigma(A_d/A^*)$ and the nozzle exit to throat area ratio, $\Sigma(A_{ne}/A^*)$. The actual $\Sigma(A_d/A^*)$ for S2c-A was 42.41. The nozzle exit-to-throat area ratio, A_{ne}/A^*, was 12.25. This increase in P_c/P_t from 0.00119 to 0.00320 for S2b-A and S2c-A indicates that the diffuser was not started for S2c-A. Only two parameters could cause this failure-to-start condition: (1) second-throat contraction area ratio, $\Sigma(A_{st}/A_d)$, and (2) the spacing of the second throat with respect to the nozzle exit. The second-throat contraction area ratio which would prevent the diffuser from starting could be too small. If the nozzle exit is too close to the beginning of the second throat, the jet impinges on the transition to the second throat so that a higher-than-minimum test cell pressure results. If the nozzle exit is too far from the beginning of the second throat, then the large mixing losses due to a long jet boundary are such that the jet boundary impingement cannot pump out of the second-throat transition. In this case the diffuser fails to start.

According to Ref. 1 and experience with other second throat ducts, the $\Sigma(A_{st}/A_d) = 0.5688$ for S2c-A was not too small and should start; therefore, the spacing of the nozzle exit with respect to the beginning of second throat was not optimum. The spacing X, could not be varied for this configuration. The three configurations (S2a-A, S2b-A, and S2c-A) had the same spacing (X = 7.50 in.), but different contraction area ratios, $\Sigma(A_{st}/A_d)$. S2b-A had a $\Sigma(A_{st}/A_d) = 0.5819$, and S2c-A had a $\Sigma(A_{st}/A_d) = 0.5688$. This small decrease in $\Sigma(A_{st}/A_d)$ was sufficient to cause S2c-A (with the set spacing between the nozzle exit and the beginning of the second throat, X = 7.50 in.) not to pump the minimum $P_c/P_t = 0.00119$ which was pumped by S2b-A. Figure 9 of Ref. 1 shows that diffusers will start with contraction area ratios much smaller than 0.5688 for a diffuser Mach number of 5.69. This is also true for data presented in this report (Table 1).

The jet boundary was calculated by the method given in Ref. 3 for S2c-A and S2b-A. The jet boundary for S2c-A impinged on the

second-throat transition near the intersection of the obround duct inlet with the transition to the second throat for the circular sides of the obround duct. The jet boundary midway between the two nozzles did not impinge on the wall of the diffuser, second throat transition, or second-throat. The jet boundary for S2b-A impinged on the duct at 3.00 in. from the nozzle exit for the circular sides of the obround duct. This jet impingement region on the diffuser wall midway between the two nozzles extended to 4.55 in. from the nozzle exit. By considering the jet impingement region location on the diffuser wall as 3.00 in. from the nozzle exit and the minor diameter (3.548 in.) as the diffuser diameter, then the non-dimensional ratio of the distance between the jet impingement on the diffuser and the beginning of the second throat to the diffuser diameter is $(7.50 - 3.00)/3.598 = 1.27$. The ratio of 1.27 for the second-throat contraction area ratio $\Sigma(A_{st}/A_d) = 0.5688$ is in agreement with the trend of the data presented in Fig. 6 of Ref. 1.

The start and operate driving pressure ratio, P_{ex}/P_t, was increased by adding a second throat. Configuration 2a-A had a $P_{ex}/P_t = 0.0307$, but when the second throat was added to form configuration S2a-A, the P_{ex}/P_t increased to 0.0374. The ratio of $(P_{ex}/P_t)_{st}/(P_{ex}/P_t)$ is 1.22, which corresponds to an $A_{st}/A_d = 0.57$ in Fig. 8a of Ref. 1. This ratio $A_{st}/A_d = 0.57$ is in agreement with the actual ratio $\Sigma(A_{st}/A_d) = 0.5744$ for S2a-A. The start and operate driving pressure ratio for S2c-A was 0.026 (Fig. 11b). The breakdown of the diffuser was gradual for S2c-A, but for the configurations (S2a-A and S2b-A), which pumped the minimum P_c/P_t, the breakdown was instantaneous. Figure 12 presents the difference in performance that was obtained for 3-A, S3a-A, and S3b-A which were smaller obround diffusers than were the configuration 2 series. The minimum ratios of P_c/P_t pumped by 3-A and S3a-A or S3b-A are almost the same value. The second-throat configurations S3a-A and S3b-A had the higher P_c/P_t which was approximately 0.00286 as compared with 0.00277 obtained for 3-a.

The improvement in P_{ex}/P_t is shown in Fig. 12. $P_{ex}/P_t = 0.0898$ for S3a-A, 0.0927 for S3b-A, and 0.0621 for 3-A. The breakdown pressure ratios, P_{ex}/P_t, for S3a-A and S3b-A are considered at the same point. (The average of 0.0898 and 0.0927 is 0.0913.) The ratio of these driving pressure ratios, $(P_{ex}/P_t)_{st}/(P_{ex}/P_t)$, is 1.47. The second throat configuration S3a-A or S3b-A has a contraction ratio, $\Sigma(A_{st}/A_d) = 0.5016$. The second throat duct was obround as well as was the inlet section. The duct details are presented in Figs. 5e and d. The only difference in S3b-A and S3a-A was that the inlet section was one inch shorter for S3b-A.

The axial position of S3a-A or S3b-A was variable during the run; therefore, the spacing of the nozzle exit with respect to the beginning

of the second throat was changed to find the limits where the diffuser would remain started and would still pump the minimum P_c/P_t.

Peculiar starting characteristics were found by varying the distance, X, between the nozzle exit and the beginning of the second throat. For a distance, X = 2.44 in., the diffuser started when the airflow was started, but the diffuser would not restart after breakdown by reducing P_{ex} (breakdown was made by increasing P_{ex}). While the diffuser was broken down and P_{ex} was low, X was changed to 2.13 in. This change in X caused the diffuser to restart. At X = 2.13 in., the diffuser would restart after breakdown only when the driving pressure, P_t, was reduced to zero and then increased. At X = 2.01 in., the diffuser would always restart by reducing P_{ex} after breakdown.

A jet-boundary curve was calculated for this second-throat configuration S3a-A or S3b-A while pumping the minimum P_c/P_t ratio. The location of the jet impingement on the duct can be determined by knowing the way the jet spreads (jet boundary curve), the radius from the centerline of the nozzle to diffuser wall (Fig. 5e), and the location of the nozzle exit with respect to the beginning of the second throat (dimension X). The location of the jet impingement region on the duct from the nozzle exit was 0.50 in. for the circular sides and increased from 0.50 to 3.24 in. on the flat sides of the diffuser with the 3.24-in. dimension occurring on the diffuser wall midway between the two nozzles. If 0.50 in. is considered as the distance from the nozzle exit to the jet impingement on the diffuser and if the minor diameter (2.065 in.) is considered as the diffuser diameter, then for the second-throat location of X = 2.01 in. the non-dimensional ratio of 0.731 is obtained. This spacing of 0.731 for a contraction ratio of 0.5016 is in agreement with the trend of the data presented in Fig. 6 of Ref. 1.

4.4 OBROUND DIFFUSER WITH SINGLE OFFSET AND CENTRICALLY LOCATED NOZZLE

Removing one of the two nozzles used in configurations 3-A and S3b-A gave configurations 3-B and S3b-B (Figs. 1, 5d, and 5e). The $\Sigma(A_d/A^*)$ was increased from 19.65 to 38.53. This factor of two larger in $\Sigma(A_d/A^*)$ for 3-B gave a ratio of P_c/P_t = 0.001049 which is less than half the ratio P_c/P_t = 0.002774 obtained by 3-A (Figs. 12 and 13). The ratio, P_{ex}/P_t, was reduced from 0.0621 for 3-A to 0.0158 for 3-B. The P_c/P_t = 0.001049 for a $\Sigma(A_d/A^*)$ = 38.53 is in good agreement with the data for an A_{ne}/A^* = 10.8 nozzle and A_d/A^* = 39.82 presented in Ref. 6, but the P_{ex}/P_t = 0.0158 is much lower than the P_{ex}/P_t value of 0.0346 obtained for the A_{ne}/A^* = 10.8 nozzle and A_d/A^* = 39.82.

The nozzle was moved to the center of the duct as shown in Fig. 1 and resulted in the new configurations 3-D and S3a-D. The performance of the configurations is presented in Fig. 13. Configuration 3-D gave a P_c/P_t = 0.001436, which is approximately one-half of the ratio P_c/P_t = 0.002774 obtained by 3-A. The ratio, P_{ex}/P_t, for 3-D is 0.0202. Configuration 3-B (configuration with offset nozzle) pumped a lower P_c/P_t (27 percent lower) than 3-D (configuration with the nozzle in the center of the duct), and 3-B started at a lower P_{ex}/P_t (by approximately 22 percent) than did 3-D. A comparison of the performance of the two configurations, 3-B and 3-D (shown in Fig. 13) with the performance of 5-A and 4a-A (Fig. 8) indicates that 3-B has a larger $\Sigma(A_d/A^*)$ than 3-D. Actually the physical ratios, $\Sigma(A_d/A^*)$, for the 3-B and 3-D configurations are equal. The configurations were identical except the position of the nozzle in the diffuser was different.

An average radius from the centerline of the nozzle to the diffuser wall for the two diffuser-ejector configurations was calculated by dividing the perimeter of the diffuser into 48 equal segments and averaging the radii from the nozzle centerline to the ends of each of the 48 circumferential segments. The average radii are 1.496 in. for 3-D and 1.753 in. for 3-B. The larger average duct radius (or diameter) for 3-B than the radius for 3-D accounts for the difference in performance shown in Fig. 13.

The second-throat configuration S3a-D gave a P_c/P_t = 0.001591 when the position of the nozzle exit from the beginning of the second throat was 3.69 in. When the second-throat diffuser duct configuration S3a-D is drawn on the jet boundary curve calculated from Ref. 3 with the beginning of the second throat 3.69 in. from the nozzle exit, the jet boundary intersects the S3a duct at 4.55 in. from the nozzle exit. This intersection is on the second-throat transition, which corresponds to a smaller duct area. The fact that the jet boundary impinged on the second-throat transition accounts for the higher P_c/P_t obtained for S3a-D as compared with that obtained for 3-D. When the diffuser was moved 0.25 in. farther downstream, the P_c/P_t obtained was 0.001436, which agrees with the P_c/P_t obtained for the 3-D configuration. At this position of 3.94 in., the jet impinges at 4.25 in. downstream of the nozzle exit, which is on the transition near the beginning of the second throat. Further movement of the second throat downstream caused the ratio P_c/P_t to increase because of the spillage of the low-energy, high-pressure air into the cell from the free-jet boundary over the inlet of the diffuser on the minor diameter sides where the nozzle was nearest the diffuser wall. This obround diffuser inlet section should be longer for this nozzle configuration D (Fig. 1) so that the jet would impinge only on the duct wall.

The second-throat configuration S3b-B (offset nozzle configuration) did not start when it was tested. The ratio, P_c/P_t, pumped by S3b-B was 0.00452. The straight duct configuration 3-B pumped a ratio, P_c/P_t, of 0.001049. The calculated jet boundary for S3b-B did not intersect the diffuser even at the second throat on the circular side farthest from the nozzle. The jet did intersect the duct approximately 0.80 in. downstream of the nozzle exit on the circular side of duct nearest the nozzle. This S3b-B might have started and pumped the minimum $P_c/P_t = 0.001049$ if the obround inlet section had been longer so that the nozzle could have been moved farther from the beginning of the second throat and the second-throat section longer so that the jet would have intersected the second-throat duct on the side farthest from the nozzle.

The ratio, P_{ex}/P_t, was increased from 0.0158 for 3-B to 0.0406 by having a 0.5016 second-throat contraction, $\Sigma(A_{st}/A_d)$. This improvement is greater than that obtained from the two-nozzle cluster configurations 3-A, S3a-A, and S3b-A. The ratio, $(P_{ex}/P_t)_{st}/P_{ex}/P_t$, for two-nozzle configurations was 1.47, and for the single offset-nozzle diffuser configuration S3b-B was 2.57.

4.5 TWIN INTERSECTING CIRCULAR DIFFUSER

The performance of duct configurations 4a and 4b with nozzle configuration A is presented in Fig. 14. Ratios of $P_c/P_t = 0.002076$ and 0.002170 were pumped by 4a-A and 4b-A, respectively. A small difference, which exists between the $\Sigma(A_d/A^*)$ for the two configurations $\Sigma(A_d/A^*) = 23.36$ for 4a-A and $A_d/A^* = 23.18$ for 4b-A accounts for part of the difference in P_c/P_t. The ratio

$$\frac{(P_c/P_t)_{\text{Isen without partition}}}{(P_c/P_t)_{\text{Isen with partition}}} = 0.9889,$$

is due to the area ratio difference. The ratio,

$$\frac{(P_c/P_t)_{\text{act without partition}}}{(P_c/P_t)_{\text{act with partition}}} = 0.9567,$$

is from the actual data. The P_{ex}/P_t for the two configurations are almost equal (0.0556 for 4a-A and 0.0537 for 4b-A).

Two contraction ratios were tested which make up the two duct configurations shown in Fig. 5g. The duct configurations S4a and S4b had contraction ratios, $\Sigma(A_{st}/A_d)$, of 0.5866 and 0.6393, respectively. The performance of these duct configurations with nozzle configuration A is

shown in Fig. 14. The $\Sigma(A_d/A^*)$ for configurations S4a-A and S4b-A are the same (22.98). Since the only difference in S4a-A and S4b-A is the duct contraction ratio, the duct contraction ratio difference is responsible for the differences in P_c/P_t and P_{ex}/P_t shown in Fig. 14. The S4a-A, with the smaller contraction ratio, $\Sigma(A_{st}/A_d) = 0.5866$, has the highest P_c/P_t (0.001882) and P_{ex}/P_t (0.0719). The corresponding ratios for S4b-A are $P_c/P_t = 0.001788$ and $P_{ex}/P_t = 0.0694$. The ratio of improvement in P_{ex}/P_t of the second-throat configuration over the straight diffuser configuration 4b-A increased with decreasing second-throat contraction ratio. The ratio of P_c/P_t of the second-throat configuration over the straight diffuser configuration 4b-A decreased with increasing second-throat contration ratio. These values are as follows:

Duct and Nozzle Configuration	$\frac{(P_{ex}/P_t)_{st}}{P_{ex}/P_t}$	$\frac{(P_c/P_t)_{st}}{P_c/P_t}$	$\Sigma\left(\frac{A_{st}}{A_d}\right)$
S4a-A	1.34	0.867	0.5866
S4b-A	1.29	0.824	0.6393

The same trend is shown in Figs. 8a and b of Ref. 1. The unusual result of this test is a decrease of about 15 percent in the ratio of P_c/P_t caused by the presence of a second throat for the S4b-A, S4a-A, and S5g-A configurations. This phenomenon was reported in Ref. 1.

The same phenomenon has been experienced for a straight diffuser with a centerbody ejector which mounted in the duct on an air foil strut. An optimum position of the centerbody with respect to the nozzle exit gave a maximum improvement in P_c/P_t of 29 percent. This improvement can be explained by the boundary layer transition location relative to reattachment as presented by Chapman, Kuehn, and Larson (Ref. 8, pp. 27 and 28). The second-throat transition triggers the flow regime from transitional to turbulent in the recompression region downstream of the reattachment point. This introduction of turbulence affects cell pressure as discussed in Ref. 8.

The diffuser configurations in Ref. 1 which produced the improvement in cell pressure ratio as a result of disturbances in the flow downstream of the jet boundary impingement point were operating at Reynolds numbers considerably smaller than those corresponding to the minimum value of the test cell pressure ratio, P_c/P_t, as reported in Ref. 9. The improvement in P_c/P_t resulting from operation at the optimum Reynolds number was 18.68 and 36.20 percent as compared to the 11.0 and 12.8 percent improvement, respectively, which resulted from second-throat installations in the same diffuser duct.

During the starting process in a cylindrical free-jet diffuser, the jet flow expands and first fills the duct at the exit. The free-jet boundary is long and, for the tests under discussion, is laminar (see Ref. 8). As the ejector action of the jet evacuates the dead-air region, the jet flow continues to expand until a condition is reached at which the low energy mass which turns back into the dead-air region from free-jet impingement equals the mass which is entrained by the free-jet. This represents the minimum ratio of P_c/P_t for the given set of flow parameters. If now the Reynolds number of the flow is increased (increased density), the boundary layer is energized and thus approaches transition. As a result, the rejected mass is smaller in magnitude and the entrainment potential of the free-jet is increased. This "double-action" causes a decrease in the pressure in the dead-air region and a further expansion of the free-jet with an associated increase in the pressure rise at impingement. This procedure continues as the Reynolds number is increased until turbulent flow exists throughout the separated region. In this process the boundary layer undergoes transition downstream of free-jet impingement; and when transition has moved upstream through the impingement zone and along the free-jet boundary to the driving nozzle exit, further increases in Reynolds number will not appreciably affect the ratio P_c/P_t.

The performance of the twin intersecting second-throat duct configuration S4a (contraction ratio, $\Sigma(A_{st}/A_d) = 0.5866$) was investigated with nozzle configurations A, B, and C. For the configurations S4a-B and S4a-C with only one nozzle, the duct opposite the nozzle was plugged. The performance for the three configurations S4a-A, S4a-B, and S4a-C is presented in Fig. 15. The nozzle configuration C had the smallest throat area or the largest $\Sigma(A_d/A^*)$; therefore, the ratio P_c/P_t should have been smaller than that obtained for configuration S4a-B. However, the ratio P_c/P_t for S4a-C is 0.002178, whereas the ratio P_c/P_t for S4a-B is 0.001981. This difference could be a result of possible leakage into the test cell. The ratio $P_c/P_t = 0.001882$ for S4a-A was even lower than the ratio P_c/P_t for either S4a-B or S4a-C. The nozzle exit was located the same distance from the beginning of the second throat (2.469 in.) for all three configurations. The ratios, P_{ex}/P_t, were nearly equal for the three configurations. The P_{ex}/P_t ratios for the configurations are as follows:

Duct and Nozzle Configuration	P_{ex}/P_t
S4a-A	0.0719
S4a-B	0.0706
S4a-C	0.0682

The jet boundary for S4a-A was calculated for the condition where the nozzle exit was positioned at the diffuser inlet or 2.469 in. from the beginning of the second throat. The impingement of the jet on the duct was 1.20 in. from the nozzle exit except on the flat side where it was 0.95 in. downstream of the nozzle exit. This was determined by the duct size (Fig. 5g) and the jet boundary. When the nozzle exit was positioned at the diffuser inlet (2.469 in. from the beginning of the second throat), the diffuser would not restart after breakdown when P_{ex} was reduced. The diffuser would restart when the driving pressure, P_t, was reduced to zero and then increased to the original value. When the nozzle exit was moved to a position 1.782 in. from the beginning of the second throat, the diffuser always restarted after breakdown when the diffuser exit pressure, P_{ex}, was reduced. The ratio of the distance from the jet impingement to the beginning of the second throat to the diffuser inlet diameter is 0.236, while the contraction ratio for S4a-A was $\Sigma(A_{st}/A_d) = 0.5866$. Since no other position was tested for S4a-A, it is not known whether the 1.782 in. distance from the nozzle exit to the beginning of the second throat is the maximum distance at which the diffuser will restart after breakdown when P_{ex} is reduced. The jet boundaries for S4b-A and S4a-A were the same. By drawing the duct in proper position on the jet boundary the intersection of the duct with the jet boundary can be determined. The impingement of the jet on the duct is 1.20 in. from the nozzle exit except on the flat side, 0.95 in. downstream of the nozzle exit. When the nozzle exit was positioned so that the distance from the nozzle exit to the beginning of the second throat was 1.75 in., the diffuser always restarted after breakdown when the diffuser exit pressure, P_{ex}, was reduced. For a distance greater than 1.75 in. from nozzle exit to beginning of second throat, the diffuser would not restart after breakdown when the exit pressure was reduced but would restart when the driving pressure, P_t, was reduced to zero and then increased to the original value. The ratio of the jet impingement distance from the beginning of the second throat to the diffuser inlet diameter for S4b-A was 0.223. The second throat contraction ratio for S4b-A was $\Sigma(A_{st}/A_d) = 0.6393$.

4.6 TWIN CIRCULAR DIFFUSER

A straight 2.065-in.-diam twin circular diffuser (Fig. 5h) was tested with nozzle configuration A. This configuration, 5-A, was the same as a single nozzle in a single duct. The performance of this configuration is presented in Figs. 8 and 16.

A second-throat configuration with the same size inlet twin ducts as configuration 5 was tested and the details are presented in Fig. 5i. A

series of configurations was derived by changing the size of the second throat and the length of the twin duct inlet.

The performance of the S5-A series is presented in Fig. 16. Configuration S5a-A did not start. The nozzle exit was approximately 6.0 in. from the beginning of the second throat. By changing nothing but the contraction area ratio, the ratio of P_c/P_t and ratio, P_{ex}/P_t, decreased with an increase in $\Sigma(A_{st}/A_d)$. This is shown in Fig. 16 for the following configurations:

Duct and Nozzle Configuration	Second Throat Contraction Ratio, $\Sigma(A_{st}/A_d)$
S5a-A	0.3115
S5b-A	0.4013
S5c-A	0.4560
S5d-A	0.5005
S5e-A	0.5496
S5f-A	0.6000

None of these configurations were pumping the minimum P_c/P_t that was obtained for 5-A. The twin duct inlets of S5f-A were decreased from 6.0 in. to 2.065 in. This configuration, S5g-A, started and pumped a ratio of P_c/P_t less than that pumped by 5-A when the distance from the nozzle exit to the beginning of the second throat was 1.815 in.

The distance from the nozzle exit to the beginning of the second throat was increased to 2.253 in. before the ratio of P_c/P_t started to increase as a result of the spillage of the high-pressure, low-energy air from the free jet boundary over the inlet of the diffuser. The diffuser restarted after breakdown at all positions tested when P_{ex} was reduced. The ratio of the start and breakdown driving pressure ratio, P_{ex}/P_t, for S5g-A to that for 5-A is 1.17. This ratio 1.17 for a $\Sigma(A_{st}/A_d)$ of 0.60 agreed well with the trend of the data presented in Fig. 8a of Ref. 1. From the jet boundary and configuration S5g diffuser size, the distance from the nozzle exit to the jet impingement on the diffuser was determined as 0.52 in. at the 2.253-in. position of the nozzle exit from the beginning of the second throat. The distance from the jet impingement on the diffuser to the beginning of the second throat was 1.733 in. The maximum distance of the jet impingement on the diffuser from the beginning of the second throat could not be determined since spillage from the free jet boundary over the diffuser inlet was evident at the 2.253-in. position at which the diffuser would continuously restart when P_{ex} was reduced after breakdown. The 1.733-in. distance from diffuser jet impingement region to the beginning of the second throat ratioed to the diffuser inlet diameter of 2.065 in. was 0.839. This ratio

of 0.839 for the 0.60 second-throat contraction ratio, $\Sigma(A_{st}/A_d)$, falls in line with data plotted in Fig. 6 of Ref. 1.

4.7 NON-SYMMETRICAL TWIN INTERSECTING CIRCULAR SECOND-THROAT DIFFUSER

The performance of the S6-C configuration is presented in Fig. 17. The nozzle exit was 3.04 in. upstream of the beginning of the second throat. The P_c/P_t pumped by S6-C configuration with nozzle exit at this position is 0.001413. The one-dimensional isentropic pressure ratio, P_c/P_t, for the $A_d/A^* = 37.76$ for S6-C is 0.001038. The ratio of these ratios, $(P_c/P_t)_{act}/(P_c/P_t)_{Isen.}$, is 1.36. The ratio, P_{ex}/P_t, is 0.0441. This diffuser was not tested without a second throat; therefore, it is not known how great an improvement in P_{ex}/P_t the second-throat contraction area ratio, $A_{st}/A_d = 0.5732$, has made. The theoretical normal shock pressure ratio, P_{ty}/P_{tx}, is 0.0414.

With the above performance and nozzle exit position, the jet boundary was calculated for S6-C configuration. At the largest radius (2.117 in.) from the centerline of the nozzle to the diffuser wall, the jet boundary intersected at a distance of 5.75 in. downstream of the nozzle exit. The second throat begins at 3.04 in. downstream of the nozzle exit for the longest radius. Since the jet boundary intersects the 2.117-in. radius farther downstream of the nozzle exit than the beginning of the second throat, it is obvious that the jet is impinging partially on the second throat transition. The impingement of the jet on a smaller area than the cross section of the diffuser inlet partially accounts for the higher P_c/P_t than the one-dimensional isentropic value based on $\Sigma(A_d/A^*)$. The shortest radius (1.008 in.) intersected the jet boundary at 0.35 in. downstream of the nozzle exit. The second throat would have to be moved away from the nozzle exit 2.71 in. for the longest portion of the jet boundary to completely impinge on the diffuser inlet. This would move the shortest portion of the jet boundary upstream of the diffuser inlet, causing a spillage of air into the cell. The spillage of the high-pressure, low-energy air would start when the second throat was moved downstream approximately 0.35 in., giving a higher cell pressure. The nozzle would be approximately 0.29 in. upstream of the diffuser inlet.

The cell pressure, P_c, increased during the test when the second throat was moved from the 3.04 in. to a 0.85 in. position from the nozzle exit because the jet boundary was impinging on a smaller area. A slight decrease in P_c was first observed and then an increase in P_c as the second throat was moved farther away from the nozzle exit (3.04 to 4.084 in.). The decrease was a result of the increased cross-sectional

area of the impingement of the jet by moving the second throat downstream. After the second throat was moved downstream greater than 0.25 in. from the 3.04 in. position toward the 4.084-in. position, a continual increase in P_c was observed because of the spillage of air into the cell where the jet boundary had moved outside the diffuser inlet at the nearest point to the nozzle. The section of the diffuser before the beginning of the second throat should have been at least 6.00 in. long. For a length of 6.00 in., the jet impingement could have been positioned in the diffuser inlet section. This would have resulted in a lower cell to driving pressure ratio, P_c/P_t.

4.8 DIFFUSER PERFORMANCE DEVIATION FROM ONE-DIMENSIONAL ISENTROPIC

The deviation of the actual cell-to-driving pressure ratio from the one-dimensional isentropic value for the different types of diffuser-ejector configurations is presented in Fig. 18. The dashed line represents the $\gamma = 1.40$ isentropic curve. The three smaller area ratio, $\Sigma(A_d/A^*)$, diffuser configurations coincided with the $\gamma = 1.40$ isentropic curve except for S5g-A and S4b-A. These two second-throat configurations had the unusual P_c/P_t performance where there was a decrease in minimum cell-to-driving pressure ratio caused by the presence of a second throat as explained in section 4.5. The four larger area ratio, $\Sigma(A_d/A^*)$, diffusers had a much higher P_c/P_t performance than the $\gamma = 1.40$ isentropic. This higher than isentropic P_c/P_t ratio trend for the diffuser configurations with area ratio, $\Sigma(A_d/A^*) > 35$, follows the trend for single nozzle in single duct presented in Fig. 9 of Ref. 6. The A_{ne}/A^* of 12.25 nozzles presented in this report corresponds more closely to the A_{ne}/A^* of 10.8 nozzle in Ref. 6.

4.9 DIFFUSER PERFORMANCE DEVIATION FROM ONE-DIMENSIONAL NORMAL SHOCK TOTAL PRESSURE RATIO

The deviation of the actual ratio, P_{ex}/P_t, from the one-dimensional normal shock value for the different types of second-throat diffuser-ejector configurations is presented in Fig. 19. All configurations except S5g-A had a start and breakdown driving pressure ratio equal to or greater than the one-dimensional normal shock value. The one-dimensional normal shock value is shown in Fig. 19 as the dashed line. The S5g-A configuration was a twin duct inlet diffuser with a common second throat. The length of the second throat-to-diameter ratio, ℓ/d, was 1.55 as compared with all the remaining second-throat configurations presented in Fig. 19, which had ℓ/d ratios greater than 4 but less than 5.

The starting and driving pressure ratio deviation from one-dimensional normal shock for the corresponding straight diffuser-ejector configurations was discussed earlier and is presented in Fig. 9. Figure 10 shows that a maximum of 90 percent of the one-dimensional normal shock total pressure ratio can be expected from straight diffuser-ejector configuration. Greater than the normal shock total pressure ratios can be accomplished by having a second-throat diffuser ejector.

4.10 DIFFUSER PERFORMANCE WITH EJECTED MASS FROM THE TEST CELL

The performance for the various configurations previously discussed has been without induced or ejected mass from the test cell. The performance of all the configurations was obtained both with and without ejected mass from the cell region. The ejected mass was pumped from the cell by the two jet pumps shown in Fig. 2. Figure 20 presents the cell-to-driving pressure ratio increase for an increase in the percent of simulated rocket mass flow ejected from the test cell region.

A tremendous improvement in P_c/P_t is shown for the configurations with $\Sigma(A_d/A^*)$ = 16.72, 19.65, and approximately 23.00. This factor of 10 improvement in P_c/P_t was accomplished by ejecting a mass of approximately 0.5 percent of the simulated rocket mass flow from the test cell. The maximum improvement in P_c/P_t for the configurations with a $\Sigma(A_d/A^*)$ in the range of 38.53 to 42.94 was approximately 6 for a 0.7 percent of the simulated rocket mass flow ejected from the cell. The maximum improvement in P_c/P_t obtainable for the area ratio, $\Sigma(A_d/A^*)$, of 72.11 was only 1.70 for a 0.4 percent of the simulated rocket mass ejected from the cell. The maximum improvement obtainable with the jet pumps decreased as the diffuser-to-nozzle throat area ratio, $\Sigma(A_d/A^*)$, increased. The curves for the configuration with $\Sigma(A_d/A^*)$ of 23.00, 42.94, and 72.11 are extended from their maximum improvement point to an improvement of approximately 10 with the same trend shown by the configurations with $\Sigma(A_d/A^*)$ of 16.72 and 19.65. Now, the relationship of the percent of the simulated rocket mass ejected from the cell, W_b/W_a, and diffuser-to-nozzle throat area ratio, $\Sigma(A_d/A^*)$, for improvements in P_c/P_t of 2, 3, 4, 5, and 10 can be obtained. This relationship is presented in Fig. 21. The five points for the diffuser area ratios, $\Sigma(A_d/A^*)$ of 16.72, 19.65, 23.00, 42.94, and 72.11, fall on a straight line. The percent of the simulated mass ejected from the test cell increased as $\Sigma(A_d/A^*)$ increased for a given improvement in P_c/P_t.

A fixed geometry jet pump, such as those used in this investigation driven by a set driving pressure, will pump a particular cell pressure for no secondary mass weight flow. The secondary pressure increased

as the secondary mass weight flow increased for the set driving pressure. For the low $\Sigma(A_d/A^*)$, the diffuser-ejector configuration had a high test cell pressure which gave the greatest difference in jet pump cell pressure for no secondary mass weight flow and the simulated rocket nozzle test cell pressure. The small $\Sigma(A_d/A^*)$ configurations also have a short jet boundary, which results in small mixing losses from interaction of the free jet boundary with low-energy air in the cell. The cell pressure difference between the jet pump and simulated rocket test cell was small for the large $\Sigma(A_d/A^*)$ configuration and large for the small $\Sigma(A_d/A^*)$ configurations when the small and large $\Sigma(A_d/A^*)$ configurations were driven by equal driving pressure. The mixing losses were greater for the large $\Sigma(A_d/A^*)$ configurations. Since the jet pump secondary pressure increased with an increase in secondary mass weight flow and since the simulated rocket test cell pressure decreased with an increase in ejected mass weight flow, a limit is reached when the two pressures are essentially equal. This limit is reached when the maximum improvement in P_c/P_t is obtained as shown in Fig. 20. The pumps used in this investigation were not large enough for the large $\Sigma(A_d/A^*)$ configuration to result in an improvement in P_c/P_t of 10.

The configurations with the diffuser inlet 1.50 in. downstream of the nozzle exit had an improvement in P_c/P_t not exceeding a value of 1.65 for large values of ejected mass flow ratios, W_b/W_a, as shown in Fig. 20. This low improvement in P_c/P_t resulted from high-pressure, low-energy air spillage over the diffuser inlet from the mixing zone into the test cell. Figure 7 was previously discussed for the condition for no-ejected mass from the test cell. Configurations 1c-A and 1a-A were spilling high-pressure, low-energy air over the inlet of the diffuser into the test cell at the nearest point from the nozzle centerline to the diffuser wall for the condition for no-ejected mass from the test cell. When the cell pressure was lowered by ejecting mass from the test cell, the jet boundary spread wider and caused more spillage of the high-pressure, low-energy air into the test cell; therefore, little improvement was realized. Configuration 1b-A had no indication of spillage of high-pressure, low-energy air into the test cell when no mass was ejected from the test cell. The jet boundary impinged on the duct 2.86 in. downstream of the nozzle exit. When mass was ejected from the test cell, the jet boundary impinged 2.32 in. from the nozzle exit or 0.82 in. downstream of the diffuser inlet. Since the jet was still impinging on the diffuser downstream of the inlet no spillage was evident. Performance for this configuration is shown in Fig. 20. The diffuser was too large for one jet pump to give much improvement.

The line representing the jet boundary for ejected mass from the test cell intersected the diffuser (2a-A) at 2.28 in. downstream of the

nozzle exit or 0.78 in. downstream of the diffuser inlet. Since the mixing zone has thickness according to Refs. 4 and 5 and since the perpendicular distance from the calculated jet boundary to the inlet of the diffuser is approximately 0.25 in., a small portion of the higher than cell pressure mixing zone air exceeding the 0.25 in. distance from the jet boundary was directed into the cell. This raised the cell pressure level. Since the 2-A diffuser configurations were the same distance from the nozzle centerline for half the diameter of each nozzle, a little spillage of low energy air into the test cell summed over this equal distance from nozzle centerline to diffuser wall resulted in a large spillage of air into the test cell. The spillage of air for the circular diffuser occurred over a small portion of the circumference of the diffuser nearest the nozzle; therefore, the jet boundary would need to spread wider for a circular diffuser with the same minimum distance from the nozzle centerline to the diffuser as the obround configuration to give a total spillage to compare with that total spillage for the obround configuration.

For the jet boundary to spread wider, the jet pumps would need to eject more mass from the test cell, but as the jet spreads wider more mass is spilled from the mixing zone into the test cell. This results in little improvement in the ratio P_c/P_t with ejected mass from the test cell over the ratio P_c/P_t without ejected mass from the test cell. This relationship is presented in Fig. 20 as the line which never exceeds a cell-to-nozzle plenum chamber pressure ratio increase of 1.65.

The second-throat configurations S2a-A and S2b-A had jet boundaries for no-ejected mass from the test cell that intersected the diffuser at approximately the same position (3.00 in.) from the nozzle exit as did the previously discussed 2a-A configuration. The jet boundary for the ejected mass from the test cell condition for S2a-A intersects the diffuser at approximately the same position (2.30 in.) as did the jet boundary for the ejected mass from the test cell condition in configuration 2a-A. Since the diffuser inlets were the same size and the jet impingements were at the same locations from the diffuser inlets for the configurations S2a-A, S2b-A, and 2a-A, then the high-pressure, low-energy air spillage into the test cell from the mixing zone mass is the same for the three configurations. No essential improvement in the ratio of P_c/P_t regardless of the ratio of $\Sigma(A_d/A^*)$ can be realized by ejecting mass from the test cell unless the diffuser inlet is far enough upstream so that the entire mixing zone of the jet boundary will be inside the diffuser.

The point in Fig. 20 for configuration S6-C which represents the improvement in the ratio of P_c/P_t by ejecting mass from the test cell,

is not a true representative point since the jet boundary for the no-ejected mass from the test cell condition impinged on the second-throat transition as discussed previously. This gave a higher P_c/P_t ratio than could be obtained. Even with this condition existing an improvement in P_c/P_t of approximately 4.75 resulted.

A method of decreasing test cell pressure for a given rocket nozzle and constant driving pressure is to increase the diffuser size (A_d/A^*). As the size of the diffuser is increased, the start and breakdown exit pressure decreases (see Fig. 8). For a given exhaust pressure, the diffuser size is limited. By the use of jet pumps to eject mass from the test cell, a lower cell pressure can be obtained with essentially no change in start and breakdown diffuser exit pressure. This interesting result is presented in Fig. 22 for configuration 5-A. The closed-symbol curve represents the ejected mass from the test cell. A factor of 10 improvement in the ratio of P_c/P_t was obtained by ejecting mass from the test cell. The ratio P_c/P_t of 0.000332 obtained for the 5-A configuration with ejected mass from the test cell could be obtained with a $\Sigma(A_d/A^*)$ of 83.57 without ejected mass from the test cell if isentropic values could be accomplished with large ducts. Figure 9 shows that the actual start and breakdown pressure ratio, P_{ex}/P_t, for the $\Sigma(A_d/A^*)$ of 83.57 is 0.0153, whereas the ratio, P_{ex}/P_t, for the small diffuser $\Sigma(A_d/A^*)$ of 16.72 is 0.0722. The small diffuser with ejected mass from the test cell would start and operate at a diffuser exit pressure almost five times as great as the large diffuser without ejected mass while still pumping the same cell pressure for a given driving pressure.

5.0 SUMMARY OF RESULTS

The results of a model investigation of a series of diffuser-ejector configurations with and without ejected mass may be summarized as follows:

1. Spillage of the high-pressure, low-energy air from the free-jet boundary into the test cell resulted in an increase in P_c/P_t ratio and a decrease in the start and operate P_{ex}/P_t ratio.
2. The obround diffuser performed better than the circular diffuser of equal cross-sectional area for the two-nozzle-cluster configuration by 24 percent in P_c/P_t and by 34.9 percent in P_{ex}/P_c.
3. A constant of 0.90 times the one-dimensional normal shock total pressure ratio was found to exist for various

cross-sectional shapes and sizes of straight diffuser ejectors without subsonic diffuser as long as the diffuser duct has an L/D = 8. When the diffuser duct L/D ratio was greater or less than 8, the constant was less than 0.90.

4. Only a small increase in P_c/P_t resulted when the obround and twin intersecting circular diffuser configurations were divided by partitions. Part of the increase in P_c/P_t was caused directly by the decrease in cross-sectional area by the addition of the partition in the diffuser. However, when the partition was extended through the second-throat S2 obround diffuser configuration, the diffuser did not start and pump the minimum P_c/P_t.

5. By inserting a second throat in the diffuser, an improvement in P_{ex}/P_t was obtained; P_{ex}/P_t increased for a given decrease in the second-throat contraction ratio, $\Sigma(A_{st}/A_d)$. The P_{ex}/P_t increased as much as 1.26 times the one-dimensional normal shock total pressure ratio.

6. The presence of a second throat (configurations S4a-A, S4b-A, and S5g-A) produced an improvement in P_c/P_t of approximately 15 percent as compared with that of the straight diffuser configurations (4a-A, 4b-A, and 5-A). The ratio of the jet impingement distance from the beginning of the second throat to the diffuser inlet diameter was varied from 0.72 to 1.00 for S4a-A, from 0.54 to 1.00 for S4b-A, and from 0.88 to 1.09 for S5g-A without affecting P_c/P_t.

7. The ratio P_c/P_t was improved by 27 percent and P_{ex}/P_t was improved by approximately 22 percent for the single nozzle configurations by moving the nozzle from the geometric center of the obround duct (configuration 3-D) to the center of one of the circular sides (configuration 3-B) resulting in an effective duct area change.

8. The performance of the small area ratio, $\Sigma(A_d/A^*)$, configurations was equal to or exceeded one-dimensional isentropic performance in P_c/P_t, whereas, the large area ratio configurations gave P_c/P_t as high as 1.62 times the isentropic value.

9. A P_c/P_t improvement ratio $\left[(P_c/P_t)_{act}/(P_c/P_t)'_{act}\right]$ as large as 10 was obtained for the small area ratio configurations $\left[\Sigma(A_d/A^*) = 16.72,\ 19.65,\ \text{and}\ 23.00\right]$ when

a mass ratio (W_b/W_a) of approximately 0.5 percent was removed from the simulated rocket test cell by use of jet pumps. The jet pumps were not large enough to eject the required amount of mass from the test cell for an improvement ratio in P_c/P_t of 10 for the large $\Sigma(A_d/A^*)$ configurations.

10. When mass was ejected from the test cell, the P_c/P_t was lowered, but the P_{ex}/P_t was unchanged. This is an advantage over the use of a large duct which will give the same P_c/P_t without ejecting mass from the test cell but will start and operate at a much lower P_{ex}/P_t ratio.

REFERENCES

1. Bauer, R. C. and German, R. C. "The Effect of Second Throat Geometry on the Performance of Ejectors without Induced Flow." AEDC-TN-61-133, November 1961.
2. Wang, C. J., Peterson, J. B., and Anderson, R. "Gas Flow Tables." GM-TR-154, March 1957.
3. Latvala, E. K. "Spreading of Rocket Exhaust Jets at High Altitudes." AEDC-TR-59-11, June 1959.
4. Gooderum, Paul B., Wood, George P., and Brevaort, Maurice J. "Investigation with an Interferometer of the Turbulent Mixing of a Free Supersonic Jet." NACA Report 963, 1950.
5. Korst, H. H., Page, R. H., and Childs, M. E. "A Theory for Base Pressures in Transonic and Supersonic Flow." University of Illinois, ME-TN-392-2, March 1955.
6. Barton, D. L. and Taylor, D. "An Investigation of Ejectors without Induced Flow." AEDC-TN-59-145, December 1959.
7. German, R. C. and Bauer, R. C. "Effects of Diffuser Length on the Performance of Ejectors without Induced Flow." AEDC-TN-61-89, August 1961.
8. Chapman, Dean R., Kuehn, Donald M., and Larson, Howard K. "Investigation of Separated Flows in Supersonic and Subsonic Streams with Emphasis on the Effect of Transition." NACA R1356, 1958.
9. Bauer, R. C. and German, R. C. "Some Reynolds Number Effects on the Performance of Ejectors without Induced Flow." AEDC-TN-61-87, August 1961.

APPENDIX I

SCALE MODEL DIFFUSER-EJECTOR APPLICATION

Model diffuser-ejector studies are valuable as a basis for predicting full-scale rocket performance. An application of how this model data can be used for predicting full-scale rocket performance is shown for a typical rocket test to be conducted in J-3 altitude test cell.

The J-3 exhaust ducting limits the maximum diameter of a diffuser to 106 in. The rocket exhaust gas ratio of specific heats is 1.26. The rocket consisted of a two-nozzle cluster. The desired cell-to-rocket-chamber pressure ratio, $P_c/P_t = 0.0005$. The one-dimensional area ratio, A_d/A^*, for this P_c/P_t and for a γ of 1.26 is 99.73 (Ref. 2).

If the duct and nozzle configuration S2a-A is chosen to be scaled up to the full-scale configuration, the procedure used is as follows:

By assuming equality in duct Mach number in the model and full-scale diffuser, then for full scale

$$M_{d\ (\text{full scale})} = M_{d\ (\text{model})} \tag{I-1}$$

$$M_{d\ (\text{model})} = 5.71 \text{ from Table 1 for S2a-A} \tag{I-2}$$

$$A_d/A^* = f(M_d, \gamma) = 137.55 \quad (\gamma = 1.26) \tag{I-3}$$

$$(P_c/P_t)_{Isen} = f(M_d, \gamma) = 0.000327 \tag{I-4}$$

$$P_{ty}/P_{tx} = f(M_d, \gamma) = 0.01284 \tag{I-5}$$

From Eqs. (I-3) and (I-5),

$$(A_{st}/A_d)_{ns} = \frac{1}{(A_d/A^*)(P_{ty}/P_{tx})} = \frac{1}{(137.55)(0.01284)} \tag{I-6}$$

$$(A_{st}/A_d)_{ns} = 0.5662$$

From model data presented in Table 1 for configuration S3a-A, the ratios are as follows:

$$\frac{(P_c/P_t)_{act}}{(P_c/P_t)_{Isen}} = 1.277 \tag{I-7}$$

$$\frac{P_{ex}/P_t}{P_{ty}/P_{tx}} = 1.025 \tag{I-8}$$

$$\frac{(A_{st}/A_d)_{act}}{(A_{st}/A_d)_{ns}} = 0.9008 \tag{I-9}$$

By assuming that these ratios for the full-scale hardware remain the same as those obtained for the model, the full-scale predicted performance is as follows:

From Eqs. (I-4) and (I-7)

$$(P_c/P_t)_{pred} = (1.277)(0.000327) = 0.000418 \tag{I-10}$$

From Eqs. (I-5) and (I-8)

$$(P_{ex}/P_t)_{pred} = (1.025)(0.01284) = 0.01316 \tag{I-11}$$

From Eqs. (I-6) and (I-9)

$$(A_{st}/A_d)_{pred} = (0.9008)(0.5662) = 0.5100 \tag{I-12}$$

This diffuser with an area ratio A_d/A^* of 137.55 is larger than is necessary for a cell-to-chamber pressure ratio $P_c/P_t = 0.0005$. If $(P_c/P_t)_{act} = 0.0005$ for the full-scale hardware, then from

$$(P_c/P_t)_{Isen} = \frac{(P_c/P_t)_{act}}{\frac{(P_c/P_t)_{act}}{(P_c/P_t)_{Isen}}} = \frac{0.0005}{1.277} = 0.0003915 \tag{I-13}$$

From Eq. (I-13)

$$A_d/A^* = f(P_c/P_t, \gamma) = 119.8 \tag{I-14}$$

and

$$(P_{ex}/P_t)_{ns} = f(P_c/P_t, \gamma) = 0.01468 \tag{I-15}$$

Then from Eqs. (I-8) and (I-15)

$$(P_{ex}/P_t)_{pred} = (1.025)(0.01468) = 0.01505 \tag{I-16}$$

From Eqs. (I-14) and (I-15)

$$(A_{st}/A_d)_{ns} = \frac{1}{(A_d/A^*)(P_{ty}/P_{tx})} = \frac{1}{(119.8)(0.01468)} = 0.5686 \tag{I-17}$$

From Eqs. (I-9) and (I-17)

$$(A_{st}/A_d)_{pred} = (0.9008)(0.5686) = 0.5122 \tag{I-18}$$

The largest symmetrical obround diffuser that can be used must have the maximum diameter of 106 in. This gives an A_d of 5263 in.^{2} for a symmetrical obround diffuser for the two nozzles. If this area, A_d, when ratioed to the total nozzle throat area, A^*, is too small to give the desired cell-to-chamber pressure ratio, $P_c/P_t = 0.0005$, then a non-symmetrical diffuser must be used to get the necessary duct area to give the required performance.

TABLE I
SUMMARY OF TEST DATA

Run No.	Duct & Nozzle Configuration		Capture Duct			Second Throat Duct		Area Ratio & Mach No.		Contraction Ratio		$\frac{(A_{st}/A_d)_{act}}{(A_{st}/A_d)_{ns}}$	Without Ejected Mass		$\frac{(P_c/P_t)_{act}}{(P_c/P_t)_{isen}}$	With Ejected Mass		$\frac{(P_c/P_t)_{act}}{(P_c/P_t)'_{act}}$	Starting, Operating Pressure Ratios		$\frac{(P_{ex}/P_t)_{act}}{(P_{ty}/P_{tx})}$
	Code	Dist, z (in.)	Diam, D (in.)	Ratio L/D	Ratio X/D	Diam, d (in.)	Ratio ℓ/d	A_d/A^*	M_d	$(A_{st}/A_d)_{act}$	$(A_{st}/A_d)_{ns}$		$\frac{(P_c/P_t)_{act}}{10^{-2}}$	$\frac{(P_c/P_t)_{isen}}{10^{-2}}$		$\frac{(P_c/P_t)'_{act}}{10^{-2}}$	W_b/W_a (%)		$(P_{ex}/P_t)_{act}$	(P_{ty}/P_{tx})	
1	1a-A	+1.50	5.288	4.54				54.82	6.04		0.6337		0.0825	0.0606	1.360	0.0529	0.537	1.560	0.0200	0.0288	0.695
6	1b-A	+1.50	6.065	3.96				72.11	6.44		0.6290		0.0662	0.0409	1.618	0.0385	0.377	1.719	0.0171	0.0220	0.777
9	1c-A	+1.50	4.680	5.13				42.94	5.70		0.6376		0.2871	0.0862	3.329	0.1763	2.747	1.628	0.0239	0.0365	0.654
21	1d-A	0	4.680	5.45				42.94	5.70		0.6376		0.1369	0.0862	1.587	0.0300	0.628	4.563	0.0295	0.0365	0.808
3 & 4	2a-A	+1.50	3.548	6.76				42.97	5.71		0.6376		0.1040	0.0861	1.207	0.0799	1.371	1.302	0.0307	0.0365	0.841
7	2b-A	+1.50	3.548	6.76				42.41	5.69		0.6378		0.1211	0.0878	1.380	0.0796	0.992	1.521	0.0302	0.0370	0.817
18 & 52	2c-A	+1.50	3.548	6.76				42.41	5.69		0.6378		0.1213	0.0878	1.382	0.0783	1.790	1.549	0.0305	0.0370	0.825
5	S2a-A	+1.50	3.548	1.69	2.11	3.548	4.03	42.97	5.71	0.5744	0.6376	0.9008	0.1100	0.0861	1.277	0.0756	1.111	1.455	0.0374	0.0365	1.025
8	S2b-A	+1.50	3.548	1.69	2.11	3.548	4.03	42.41	5.69	0.5819	0.6378	0.9123	0.1194	0.0878	1.360	0.0782	1.107	1.527	0.0368	0.0370	0.995
19	S2c-A	+1.50	3.548	1.69	2.11	3.548	4.03	42.41	5.69	0.5688	0.6378	0.8919	0.3201	0.0878	3.647	0.3130	9.620	1.023	0.0300	0.0370	0.811
42	3-A	0	2.065	5.81				19.65	4.70		0.6538		0.2774	0.2688	1.032	0.0291	0.495	9.533	0.0621	0.0778	0.798
34	3-B	0	2.065	5.81				38.53	5.56		0.6395		0.1049	0.1008	1.040	0.0306	0.587	3.428	0.0158	0.0406	0.389
40	3-D	0	2.065	5.81				38.53	5.56		0.6395		0.1436	0.1008	1.424	0.0320	0.576	4.488	0.0202	0.0406	0.498
45, 46, & 47	S3a-A	-2.13—+0.31	2.065	2.06	1.03—2.21	2.065	4.84	19.65	4.70	0.5016	0.6538	0.7671	0.2804	0.2688	1.043	0.0274	0.433	10.234	0.0898	0.0778	1.154
50	S3b-A	-1.31—-0.63	2.065	1.58	1.27—0.94	2.065	4.84	19.65	4.70	0.5016	0.6538	0.7671	0.2857	0.2688	1.063	0.0290	0.975	9.852	0.0927	0.0778	1.191
51	S3b-B	-0.06—+1.25	2.065	1.58	1.54—2.18	2.065	4.84	38.53	5.56	0.5016	0.6395	0.7842	0.4520	0.1008	4.483	0.0495	1.524	9.131	0.0406	0.0406	1.000
48 & 49	S3a-D	-2.13—-0.56	2.065	2.06	1.15—1.79	2.065	4.84	38.53	5.56	0.5016	0.6395	0.7842	0.1591	0.1008	1.577	0.0260	0.698	6.119	0.0511	0.0406	1.259
13	4a-A	-0.88	2.469	10.68				23.36	4.92		0.6497		0.2076	0.2087	0.995	0.0267	0.517	7.775	0.0556	0.0659	0.844
23	4b-A	-0.88	2.469	10.68				23.18	4.91		0.6498		0.2170	0.2111	1.028	0.0350	0.550	6.200	0.0537	0.0664	0.809
36	S4a-A	-0.69—0	2.469	1.00	0.72—1.00	1.854	4.36	22.98	4.90	0.5866	0.6501	0.9024	0.1882	0.2138	0.880	0.0406	0.442	4.635	0.0719	0.0670	1.074
39	S4b-A	-1.22—0	2.469	1.00	0.51—1.00	1.936	4.28	22.98	4.90	0.6393	0.6501	0.9835	0.1788	0.2138	0.836	0.0406	0.425	4.404	0.0694	0.0670	1.036
33	S4a-B	0	2.469	1.00	1.00	1.854	4.36	22.53	4.87	0.5866	0.6505	0.9017	0.1981	0.2200	0.900	0.0299	0.527	6.625	0.0706	0.0682	1.035
35	S4a-C	-0.13—+0.63	2.469	1.00	0.95—1.25	1.854	4.36	23.44	4.92	0.5866	0.6496	0.9031	0.2178	0.2076	1.049	—	—	—	0.0682	0.0657	1.038
10	5-A	-0.88	2.065	12.77				16.72	4.51		0.6582		0.3335	0.3407	0.979	0.0332	0.418	10.045	0.0723	0.0909	0.796
12	S5a-A	0	2.065	2.91	2.91	1.630	1.24	16.72	4.51	0.3115	0.6582	0.4733	13.5550	0.3407	39.783	0.7398	22.730	18.323	—	0.0909	—
14	S5b-A	-0.72—+0.38	2.065	2.91	2.56—3.09	1.850	1.37	16.72	4.51	0.4013	0.6582	0.6097	8.3357	0.3407	24.465	0.6300	20.420	13.231	0.0946	0.0909	1.041
15	S5c-A	-0.81—+0.50	2.065	2.91	2.51—3.15	1.972	1.44	16.72	4.51	0.4560	0.6582	0.6928	5.4625	0.3407	16.032	0.6100	19.690	8.955	0.0500	0.0909	0.550
16	S5d-A	-0.81—+0.44	2.065	2.91	2.51—3.12	2.066	1.48	16.72	4.51	0.5005	0.6582	0.7604	4.0920	0.3407	12.010	0.5150	16.770	7.946	0.0450	0.0909	0.495
17	S5e-A	-0.81—+0.38	2.065	2.91	2.51—3.09	2.165	1.52	16.72	4.51	0.5496	0.6582	0.8350	3.1750	0.3407	9.319	0.4200	14.470	7.560	0.0370	0.0909	0.407
20	S5f-A	-0.81—+0.50	2.065	2.91	2.51—3.15	2.262	1.55	16.72	4.51	0.6000	0.6582	0.9115	2.1273	0.3407	6.243	0.3400	11.550	6.257	0.0296	0.0909	0.326
41	S5g-A	-0.25—+0.19	2.065	1.00	0.88—1.09	2.262	1.55	16.72	4.51	0.6000	0.6582	0.9115	0.2698	0.3407	0.792	0.0299	0.268	9.023	0.0843	0.0909	0.928
37 & 38	S6-C	-2.25—+0.98	3.826	0.81	0.22—1.07	2.326	4.65	37.76	5.54	0.5732	0.6400	0.8958	0.1413	0.1038	1.361	0.0295	0.548	4.790	0.0441	0.0414	1.065

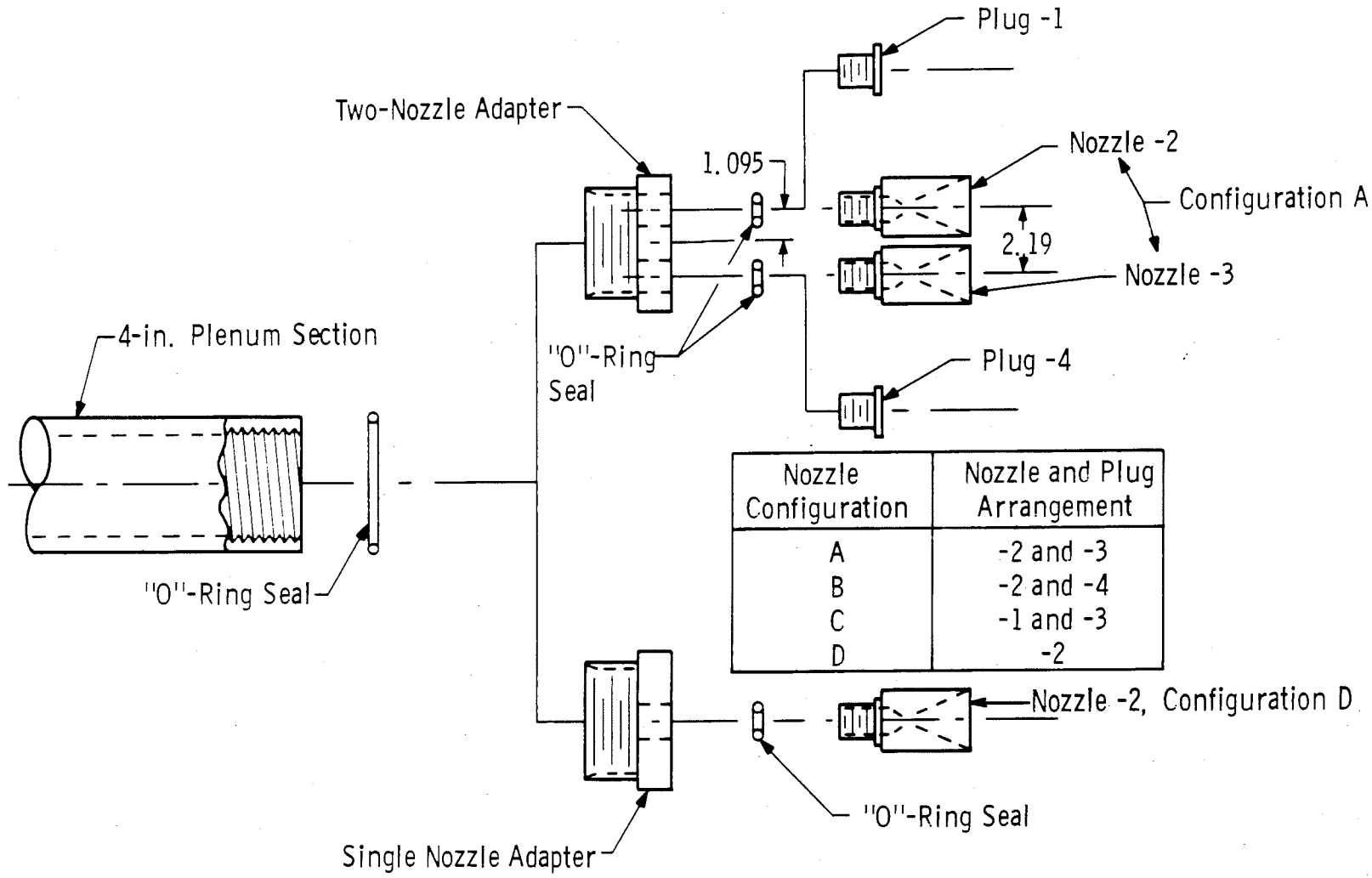

Nozzle Configuration	Nozzle and Plug Arrangement
A	-2 and -3
B	-2 and -4
C	-1 and -3
D	-2

Fig. 1 Simulated Rocket Nozzle Configurations

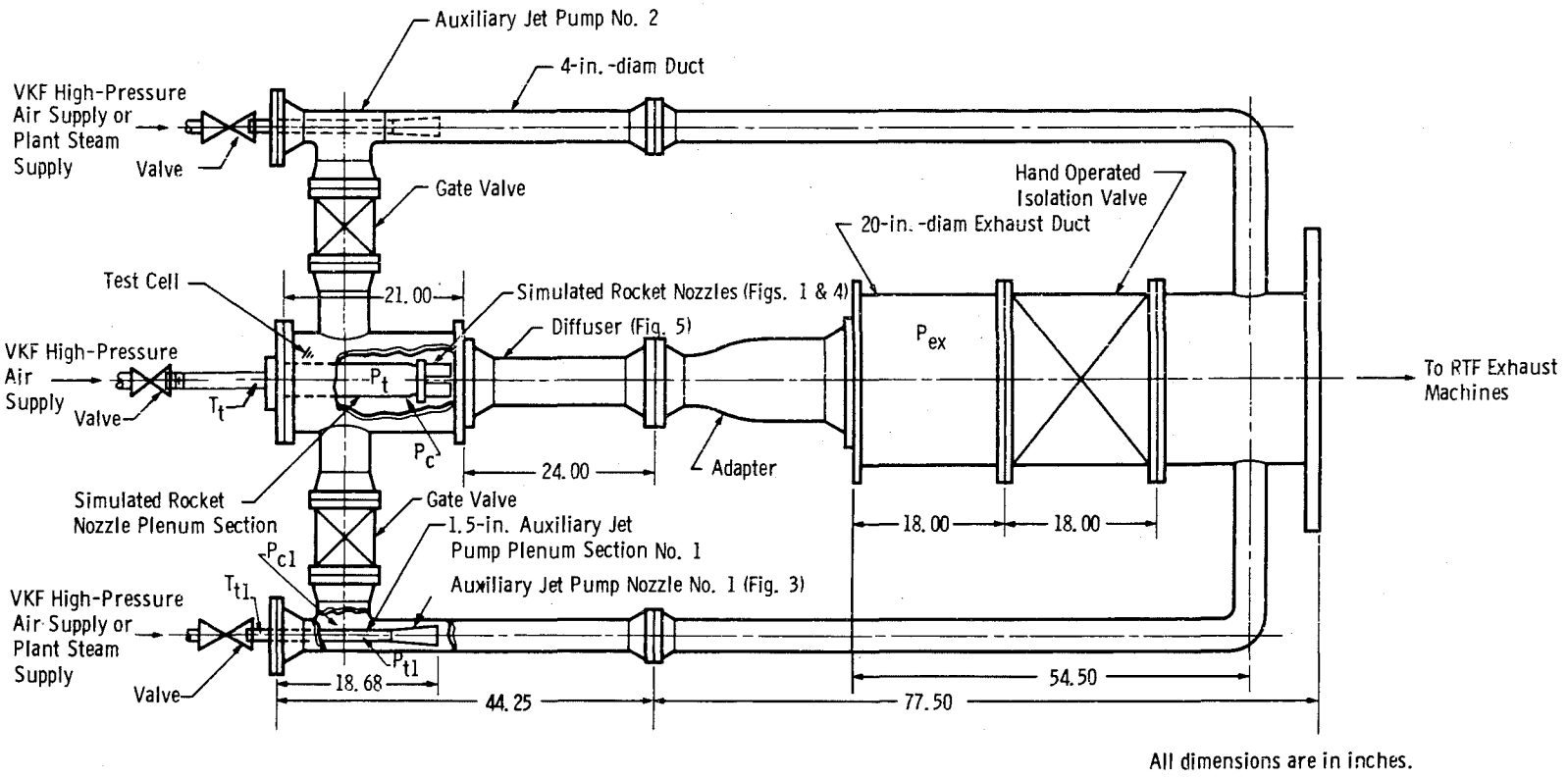

Fig. 2 T5BR-1 Test Installation

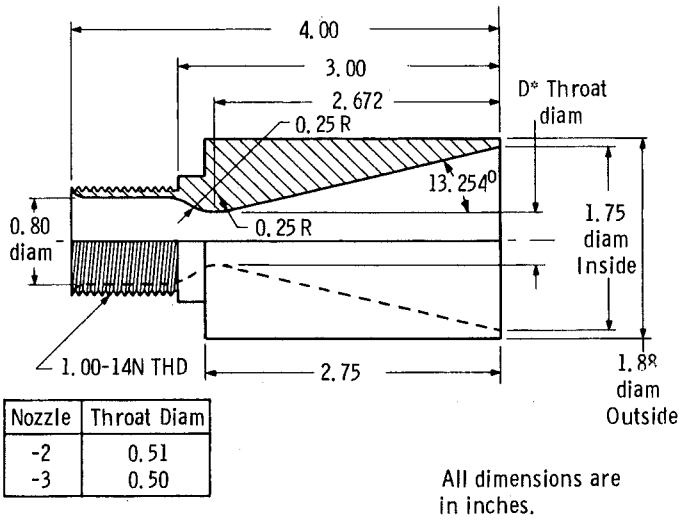

Nozzle	Throat Diam
-2	0.51
-3	0.50

Fig. 3 Simulated Rocket Nozzle Details

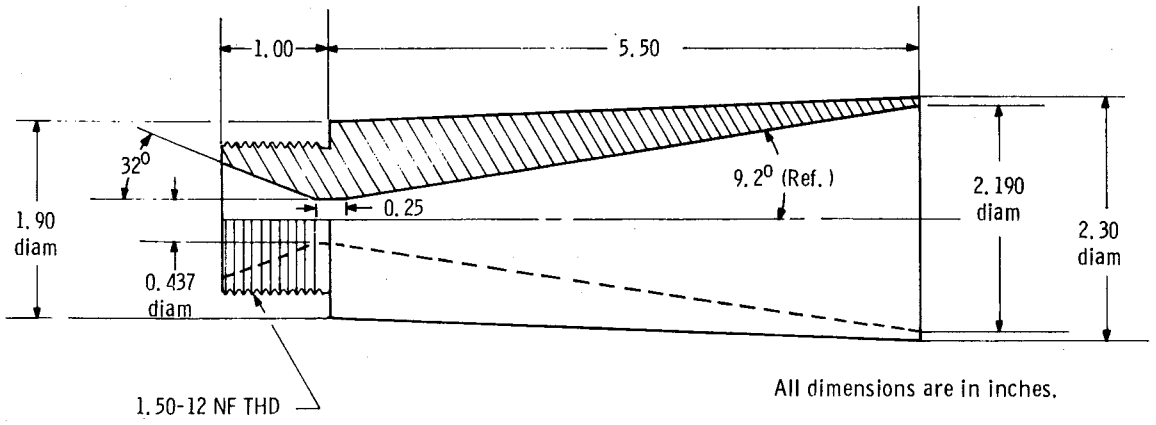

Fig. 4 Auxiliary Jet Pump Nozzle Details

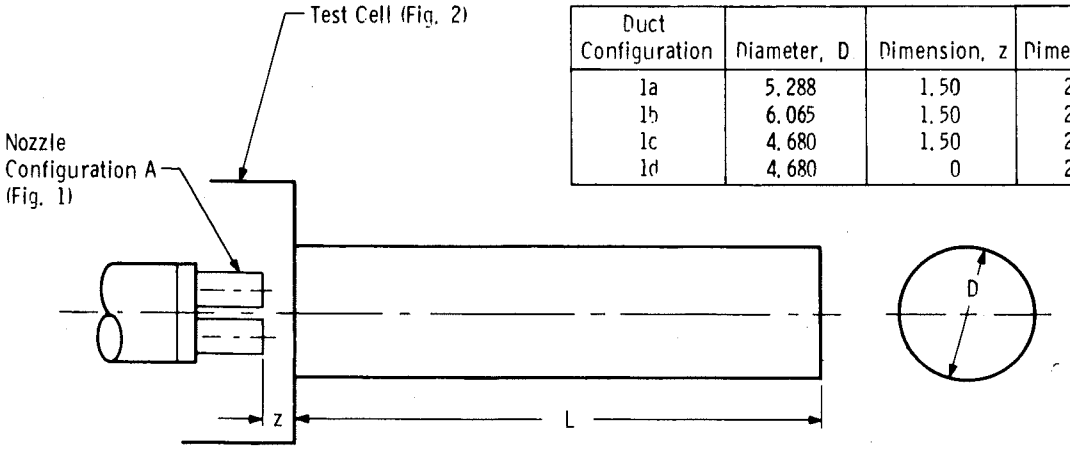

Duct Configuration	Diameter, D	Dimension, z	Dimension, L
1a	5.288	1.50	24.00
1b	6.065	1.50	24.00
1c	4.680	1.50	24.00
1d	4.680	0	25.50

All dimensions are in inches.

a. Single Straight Circular Diffuser Configuration 1

Fig. 5 Schematic of Diffuser Details

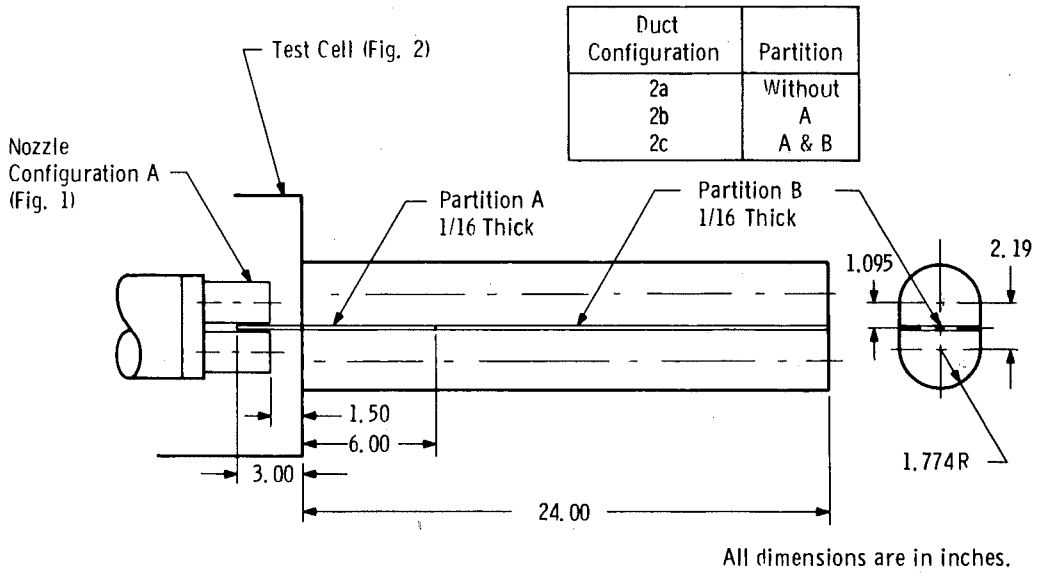

b. Straight Obround Diffuser Configuration 2

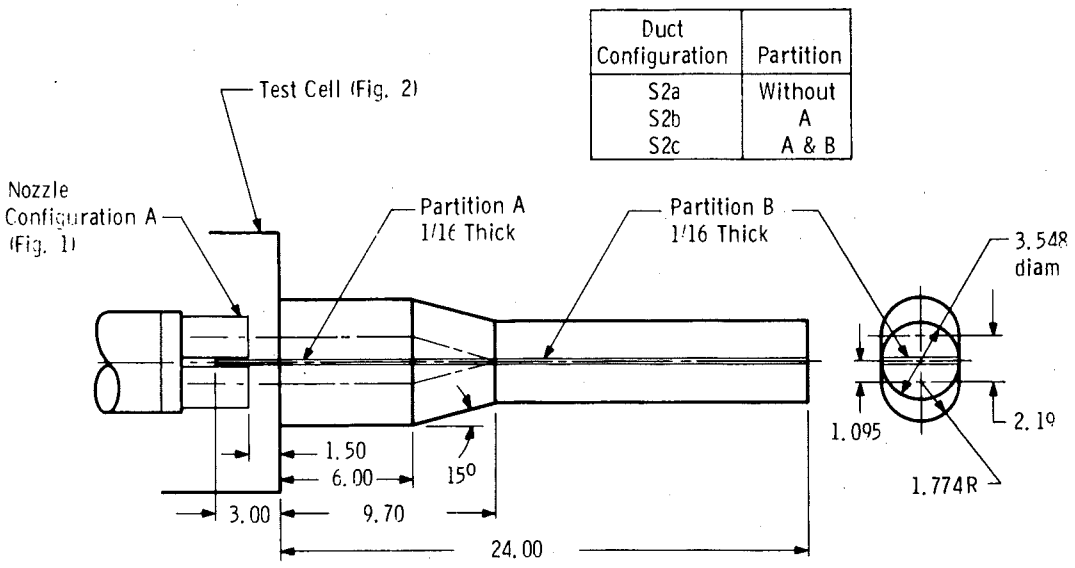

c. Second-Throat Obround Diffuser Configuration S2

Fig. 5 Continued

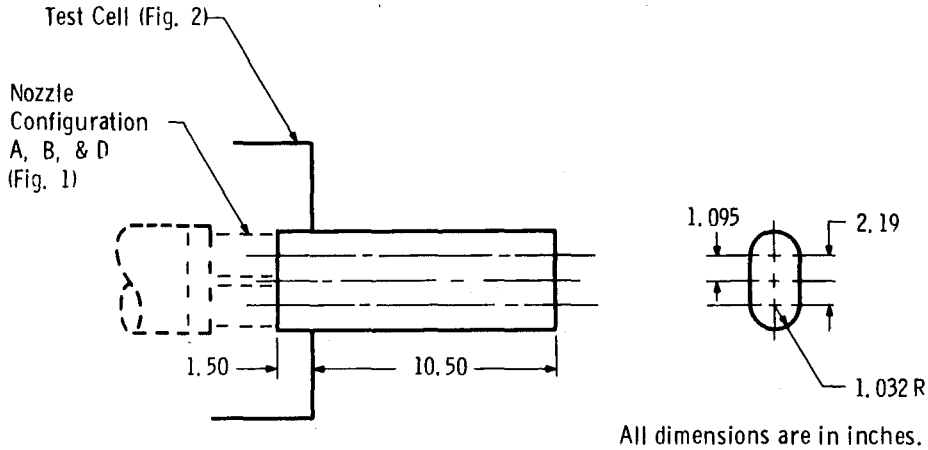

All dimensions are in inches.

d. Straight Obround Diffuser Configuration 3

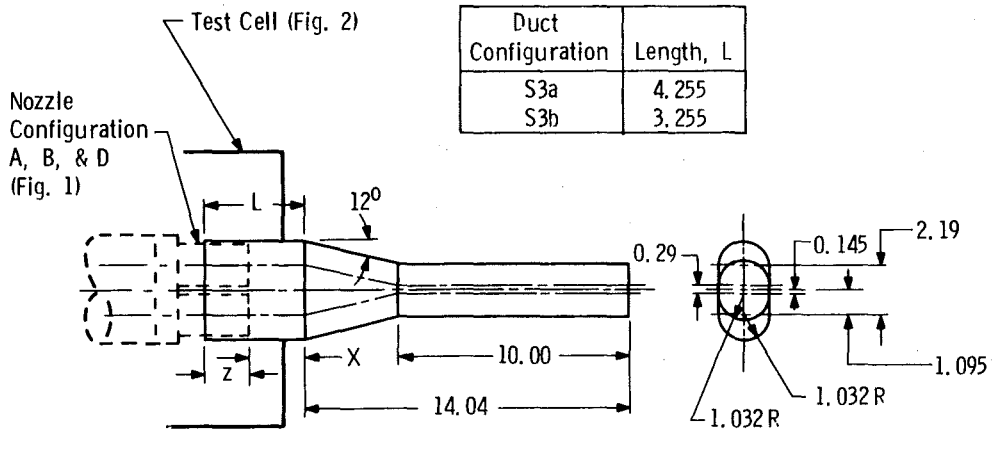

Duct Configuration	Length, L
S3a	4.255
S3b	3.255

e. Second-Throat Obround Diffuser Configuration S3

Fig. 5 Continued

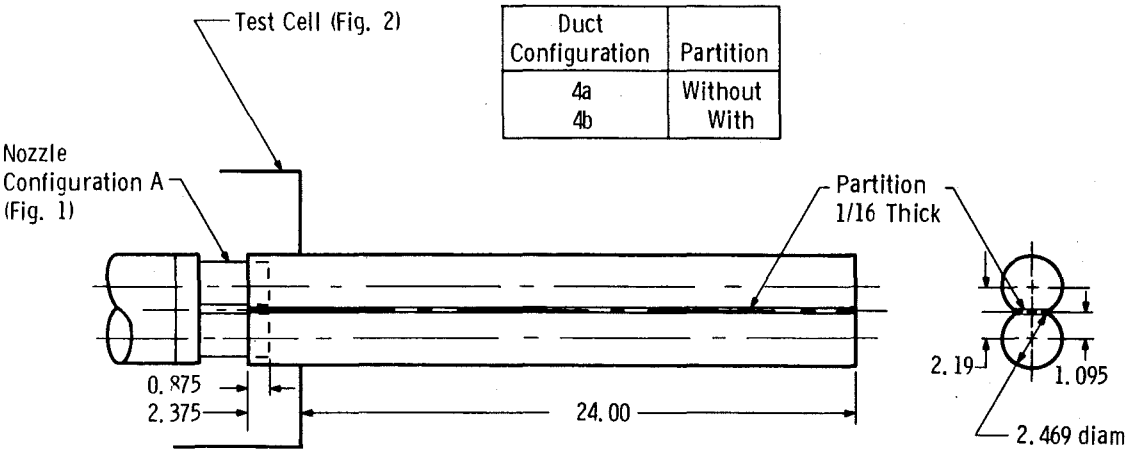

Duct Configuration	Partition
4a	Without
4b	With

All dimensions are in inches.

f. Straight Twin Intersecting Circular Diffuser Configuration 4

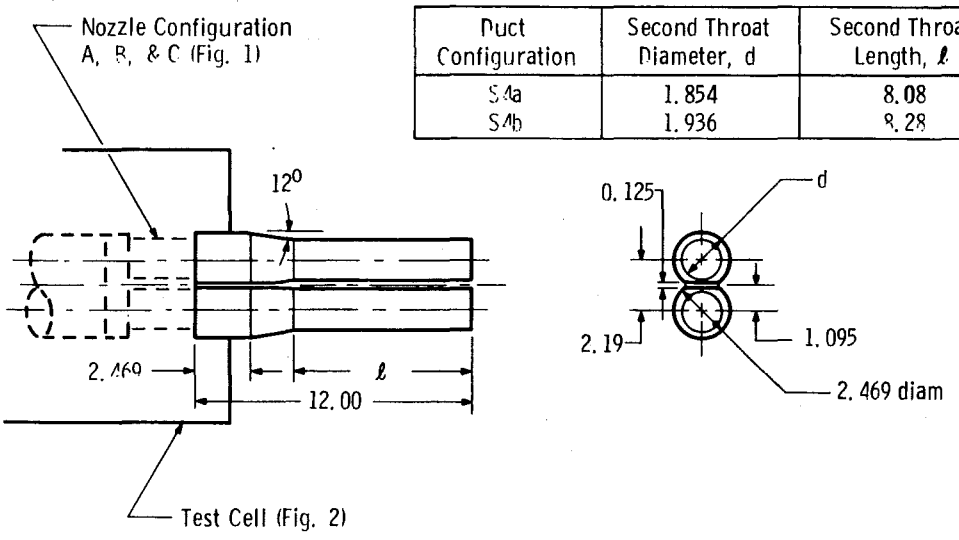

Duct Configuration	Second Throat Diameter, d	Second Throat Length, ℓ
S4a	1.854	8.08
S4b	1.936	8.28

g. Second-Throat Twin Intersecting Circular Diffuser Configuration S4

Fig. 5 Continued

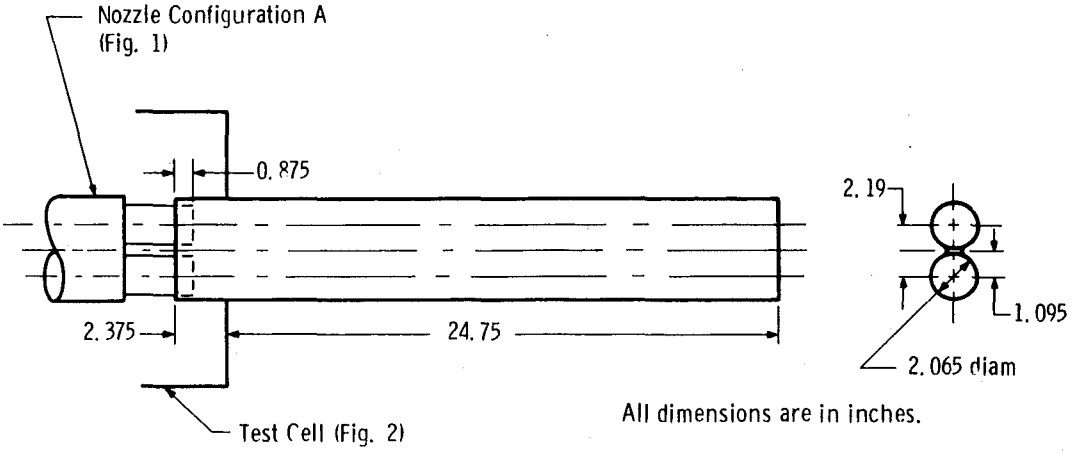

h. Straight Twin Circular Diffuser Configuration 5

Duct Configuration	Second Throat Length, ℓ	Second Throat Diameter, d	Diffuser Inlet Length, L	Diffuser Length, B
S5a	2.03	1.630	6.0	14.2
S5b	2.55	1.850	6.0	14.2
S5c	2.83	1.972	6.0	14.2
S5d	3.06	2.066	6.0	14.2
S5e	3.29	2.165	6.0	14.2
S5f	3.52	2.262	6.0	14.2
S5g	3.52	2.262	2.065	10.265

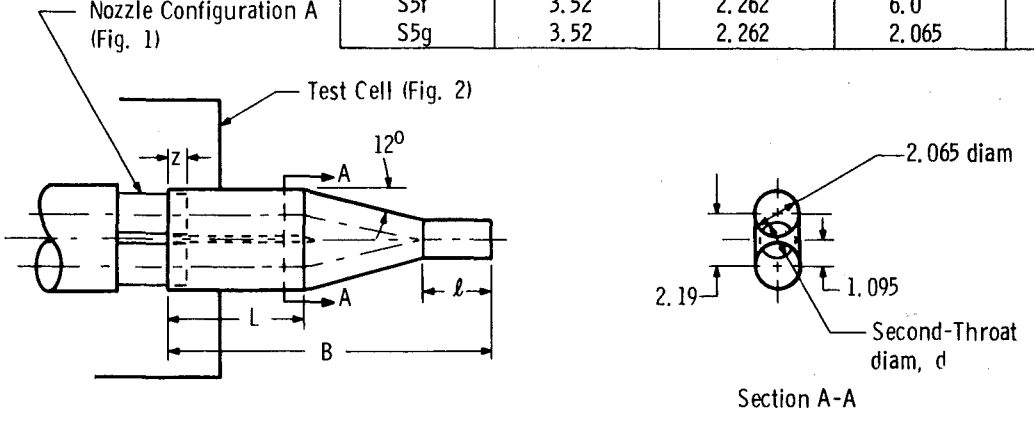

i. Twin Duct Inlet with Common Second-Throat Diffuser Configuration S5

Fig. 5 Continued

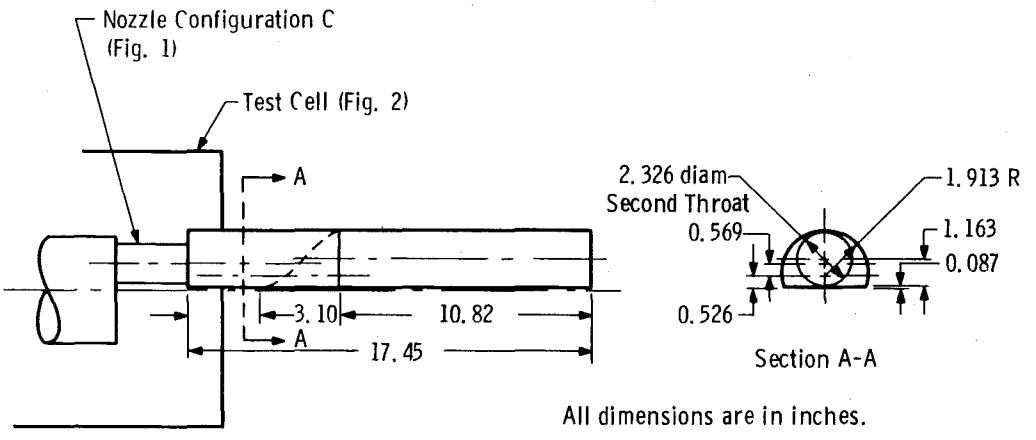

j. Second-Throat Half-Twin Intersecting Circular Diffuser Configuration S6

Fig. 5 Concluded

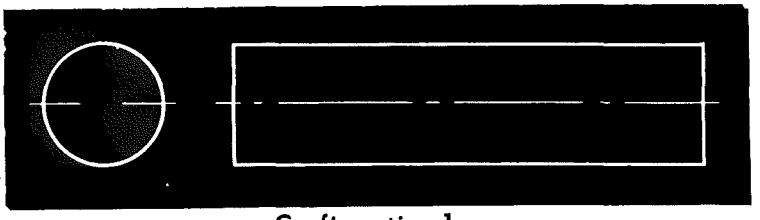

Configuration 1

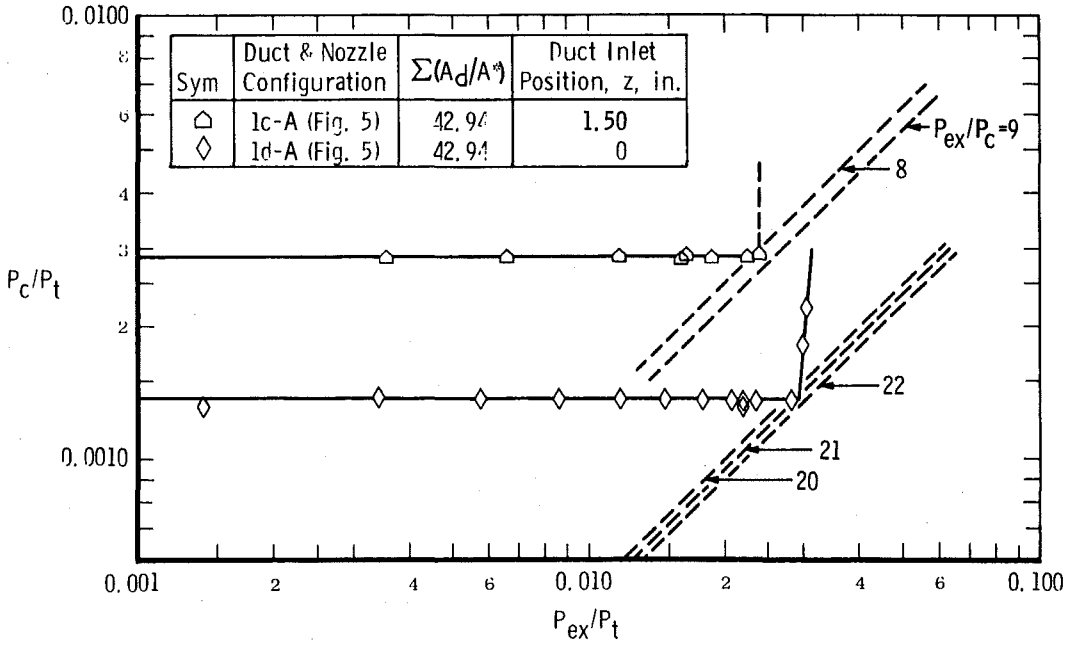

Fig. 6 Performance of Diffuser-Ejector 1c-A and 1d-A Configurations

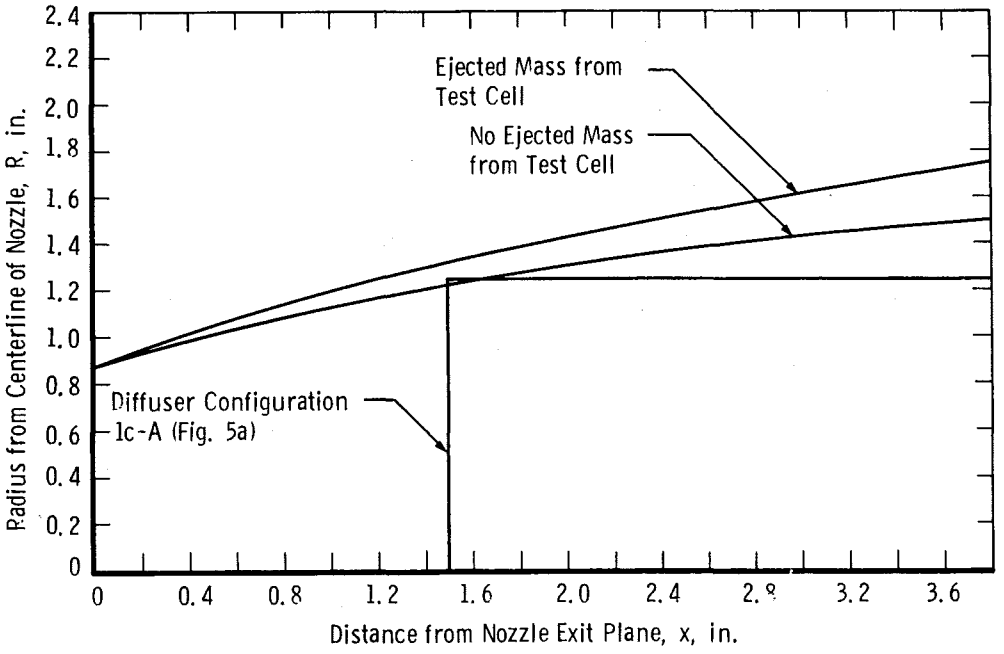

Fig. 7 Typical Jet Boundary with and without Ejected Mass from Test Cell

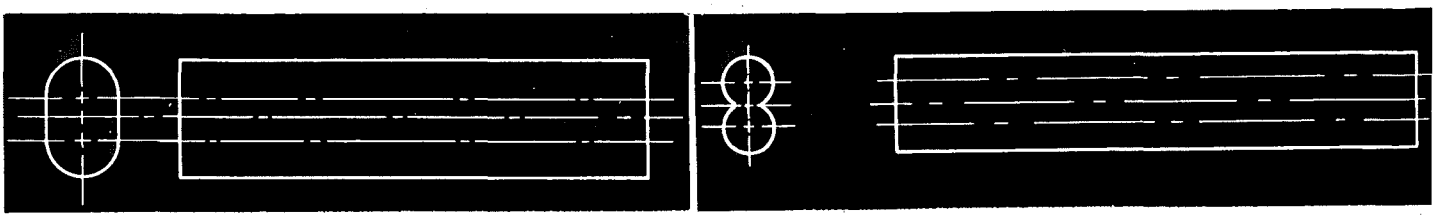

Configuration 2

Configuration 4

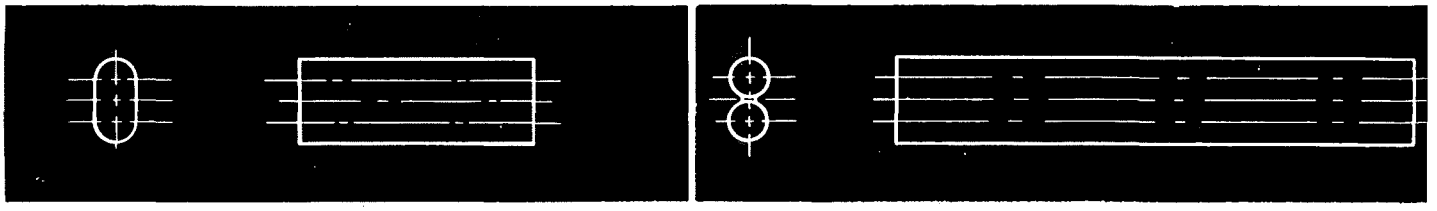

Configuration 3

Configuration 5

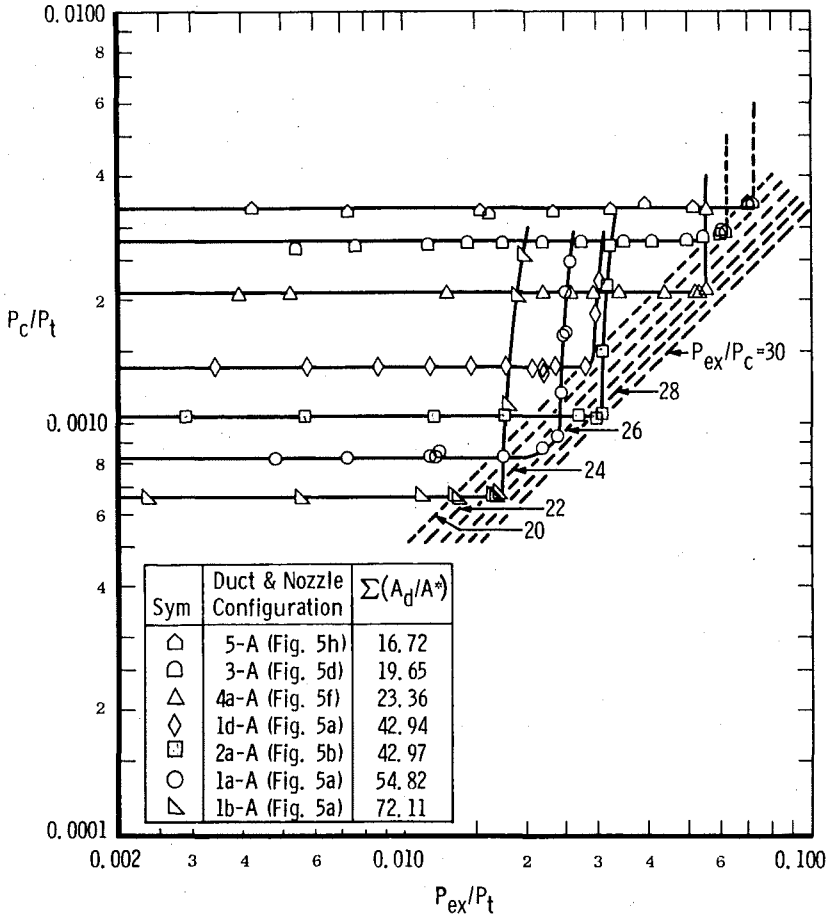

Fig. 8 Performance of Straight Diffuser-Ejector Configurations

Configuration 1

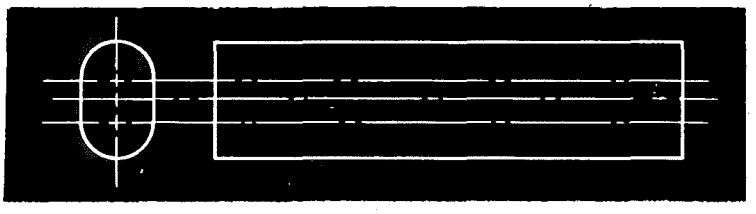

Configuration 2

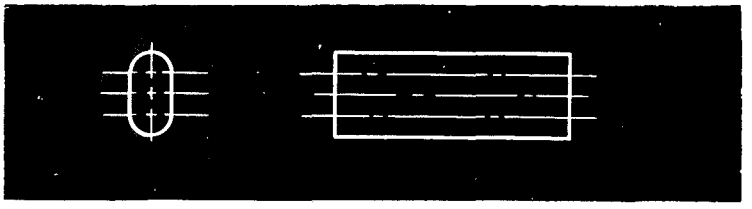

Configuration 3

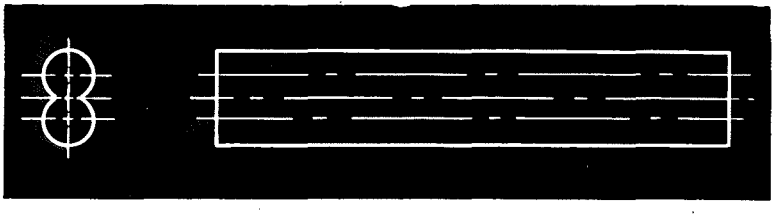

Configuration 4

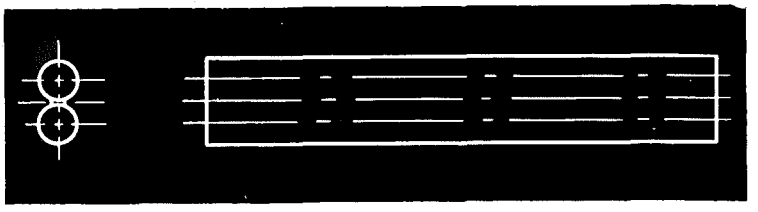

Configuration 5

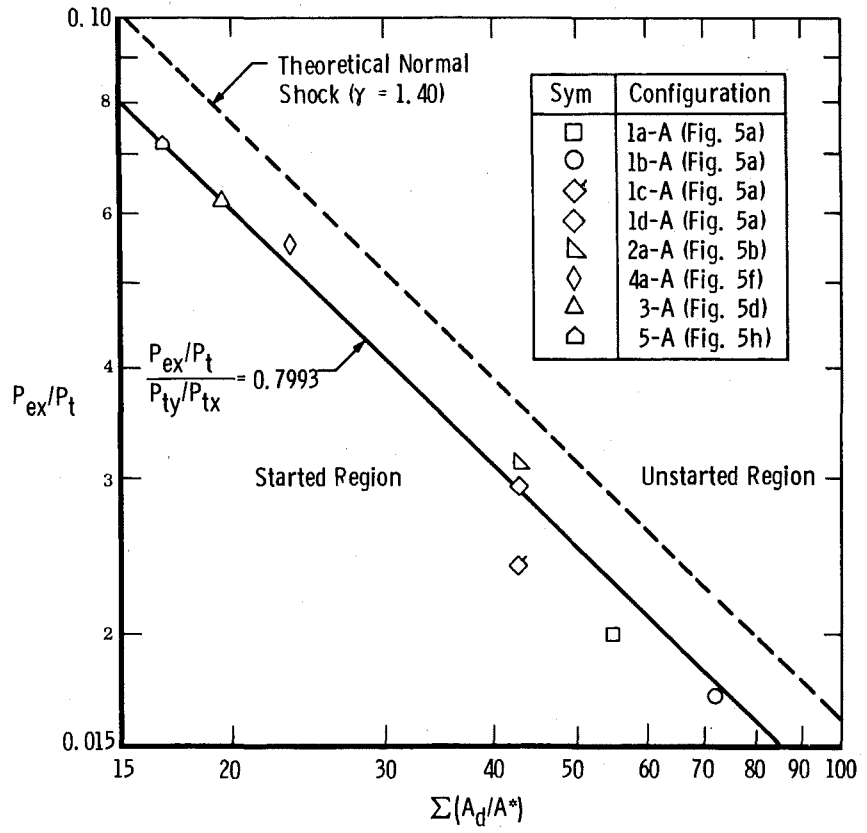

Fig. 9 Straight Diffuser-Ejector Average Pressure Ratio Required for Starting

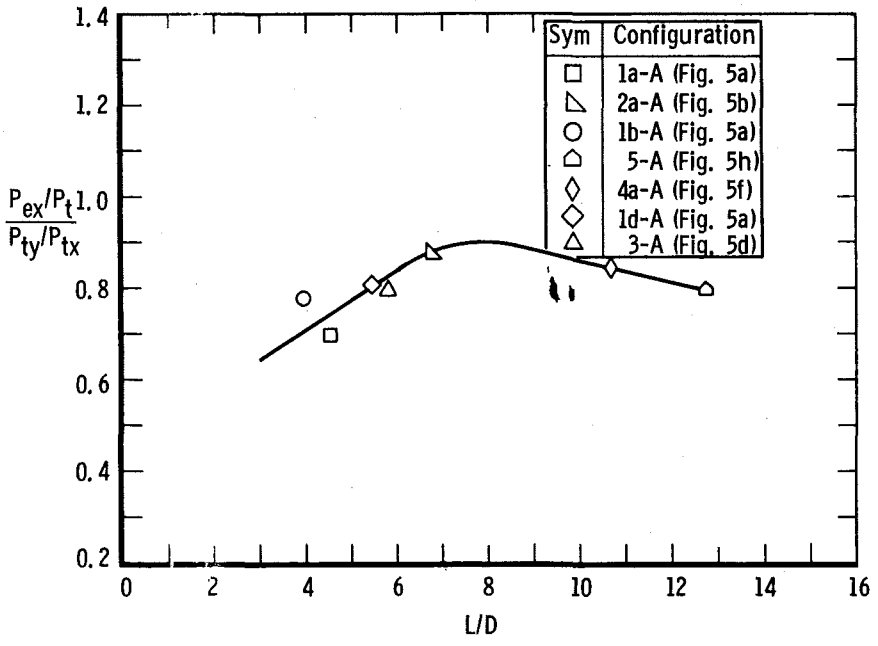

Fig. 10 Straight Diffuser-Ejector Starting Pressure Ratio Deviation from Normal Shock

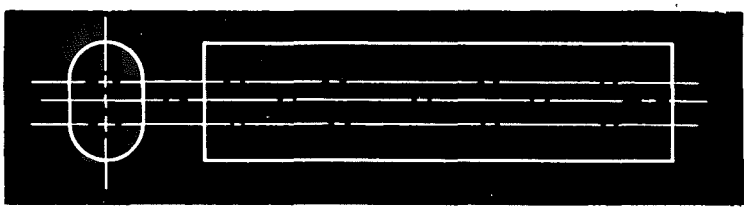

Configuration 2

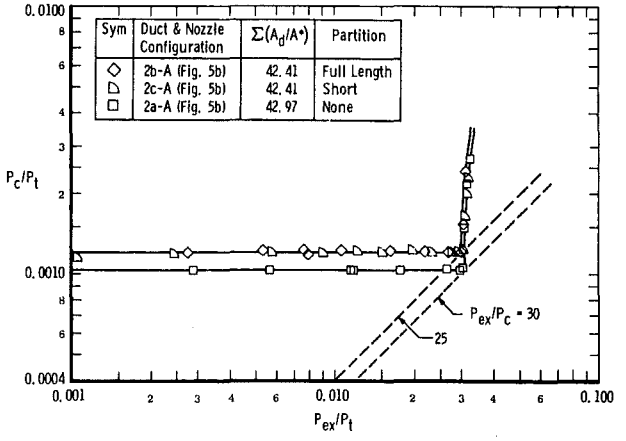

a. Straight Obround Diffuser

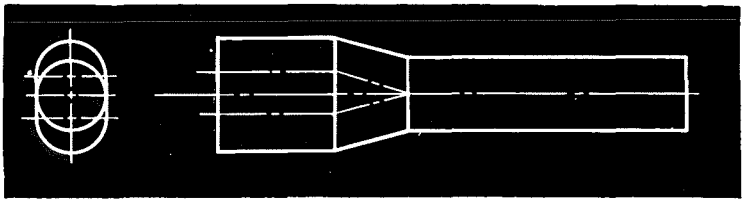

Configuration S2

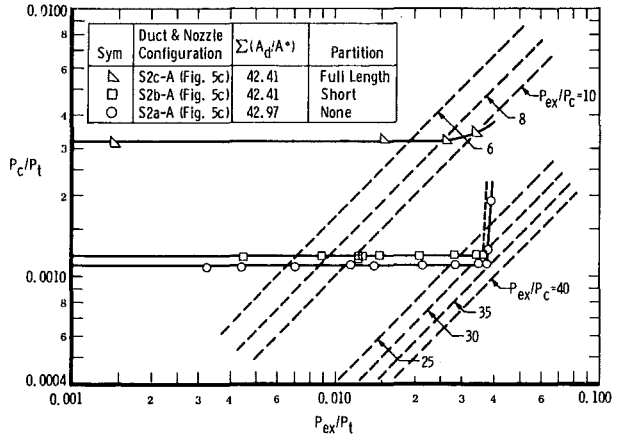

b. Second-Throat Obround Inlet Diffuser

Fig. 11 Change in Performance by Dividing the Diffuser by a Partition

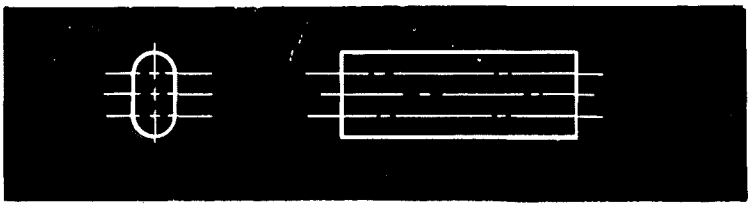

Configuration 3

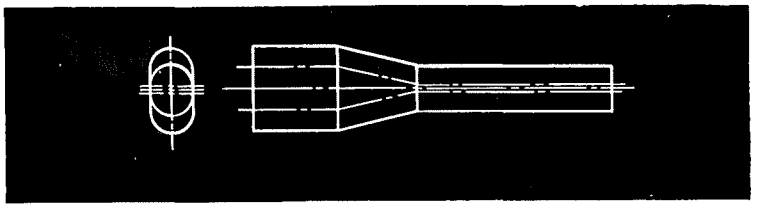

Configuration S3

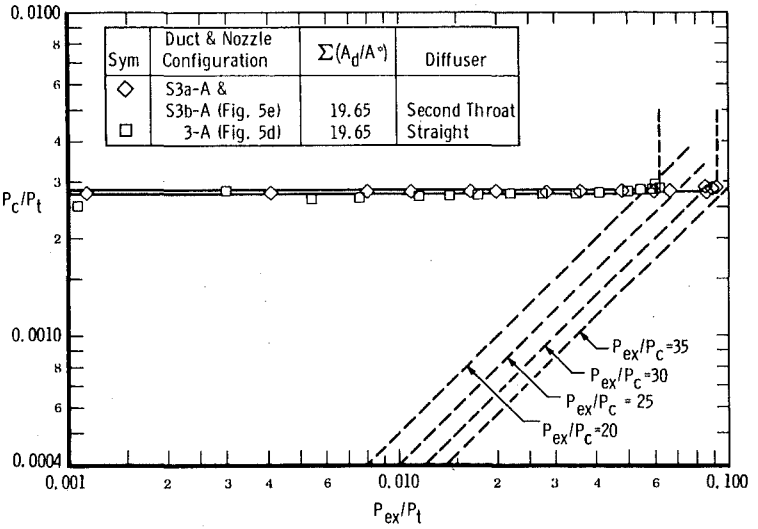

Fig. 12 Driving Pressure Ratio, P_{ex}/P_t, Improvement with Second-Throat Obround Diffusers S3a-A and S3b-A, over Straight Diffuser, 3-A

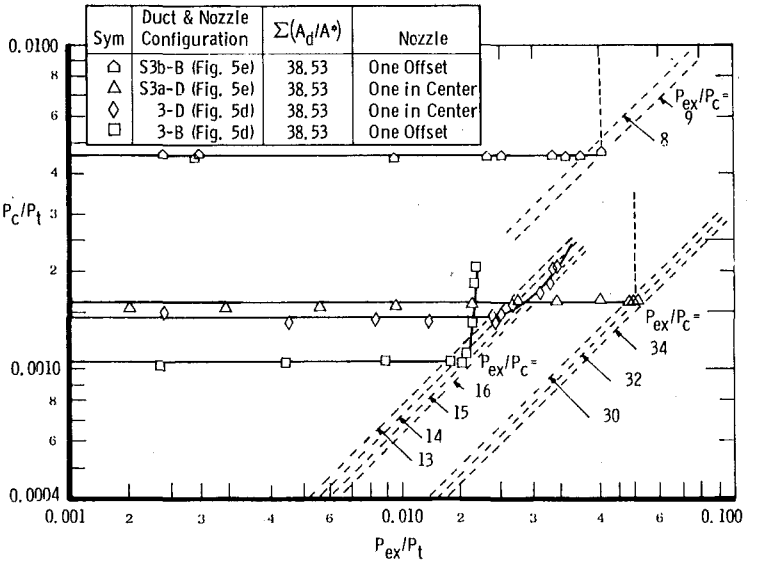

Fig. 13 Change in Performance by Changing the Radial Position of the Nozzle in Both Straight and Second-Throat Diffusers

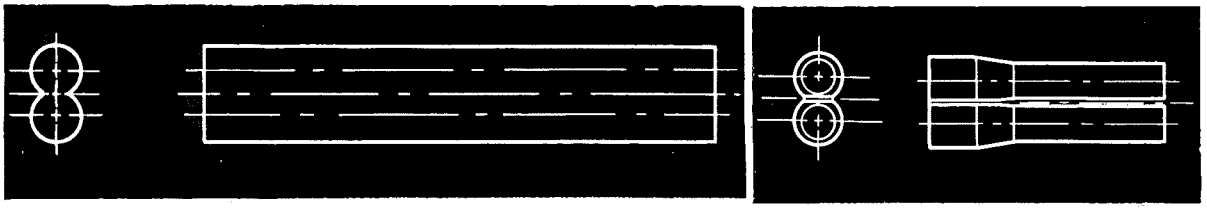

Configuration 4 Configuration S4

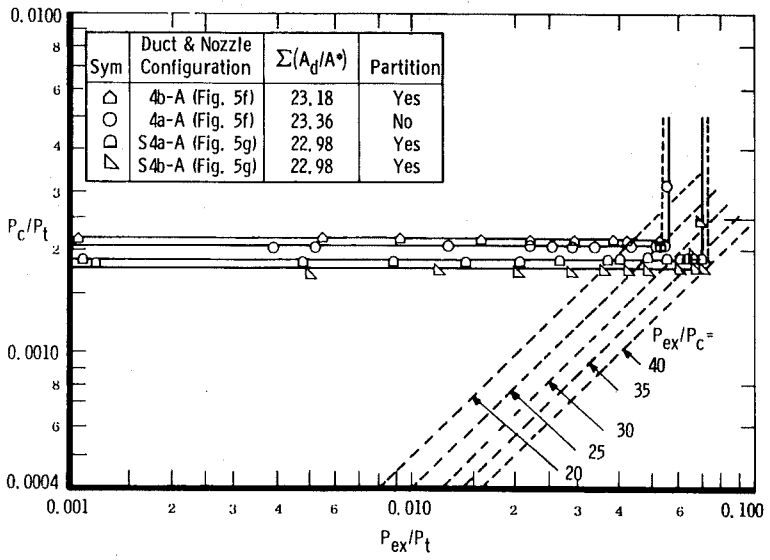

Fig. 14 Change in Performance of Twin Intersecting Circular Diffuser by Adding a Partition and Second Throat

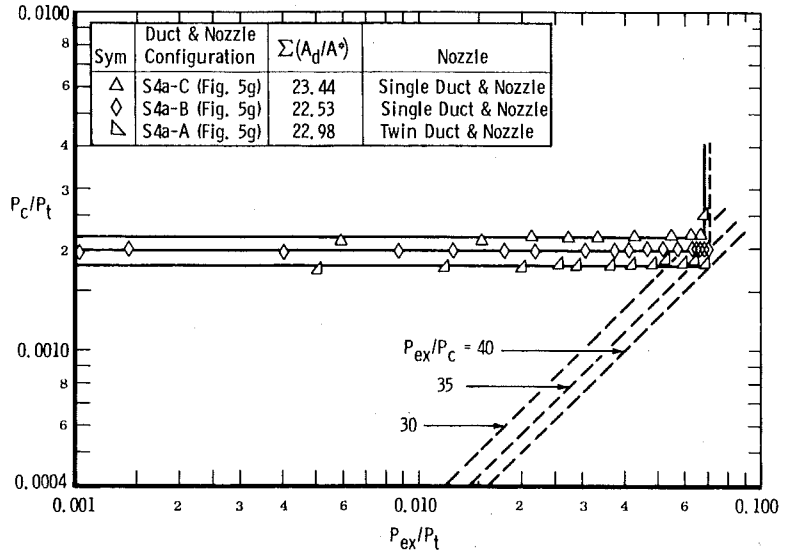

Fig. 15 Change in Performance of the Individual Duct and Nozzle Configurations, S4a-B and S4a-C, from that of the S4a-A Configuration

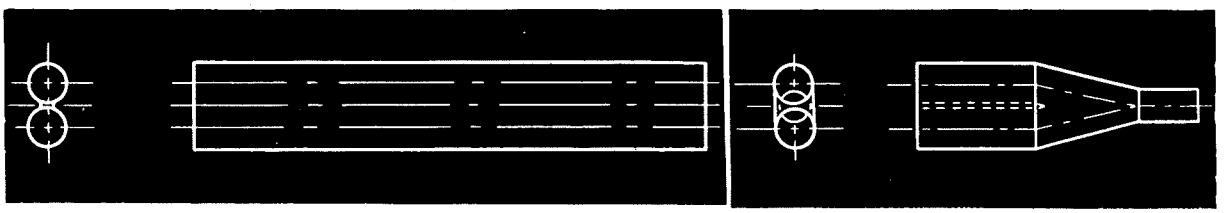

Configuration 5 Configuration S5

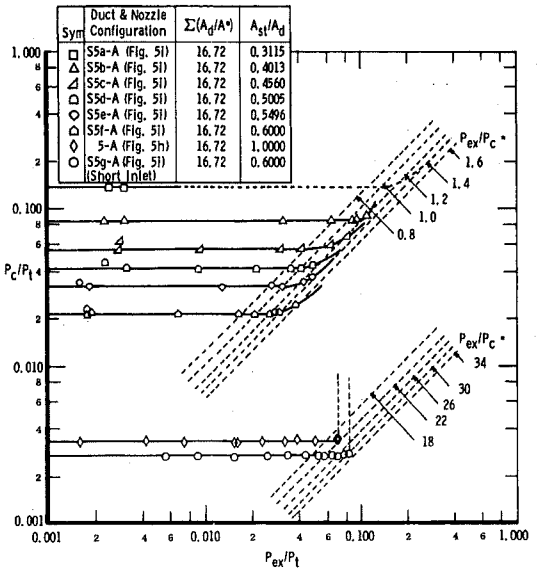

Fig. 16 Performance of Straight Twin Duct and Twin Duct Inlet with Common Second-Throat Diffusers

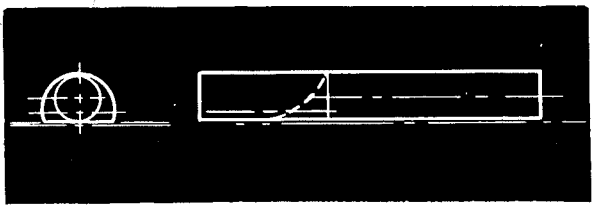

Configuration S6

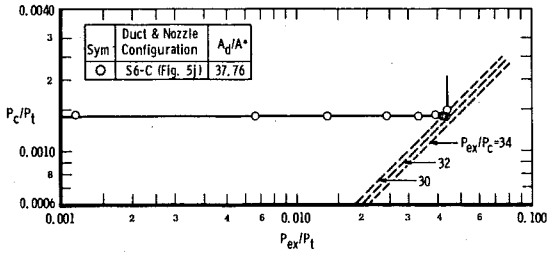

Fig. 17 Performance of Half-Twin Intersecting Circular Second-Throat Diffuser Configuration S6-C

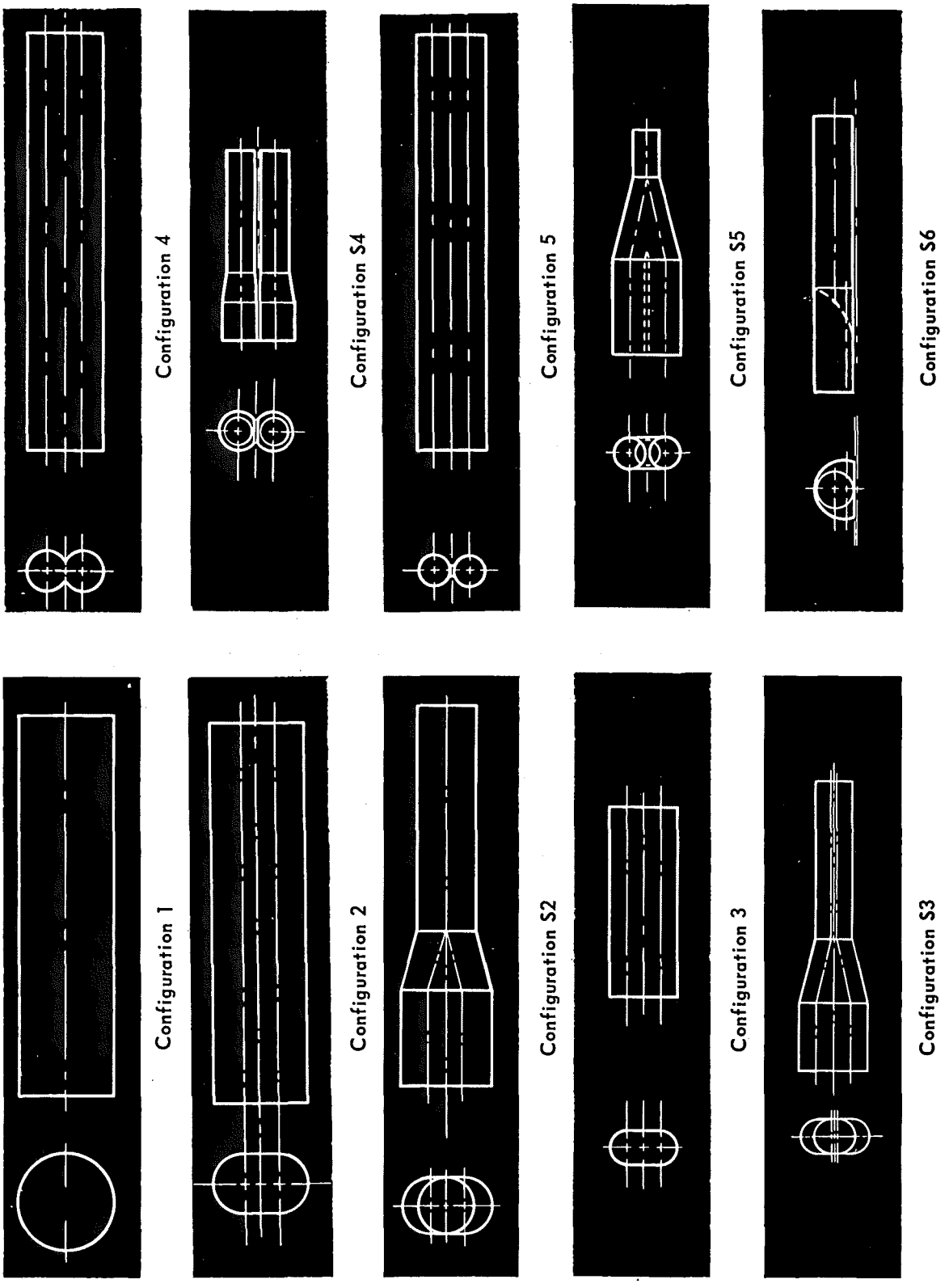
Configuration 1
Configuration 2
Configuration S2
Configuration 3
Configuration S3
Configuration 4
Configuration S4
Configuration 5
Configuration S5
Configuration S6

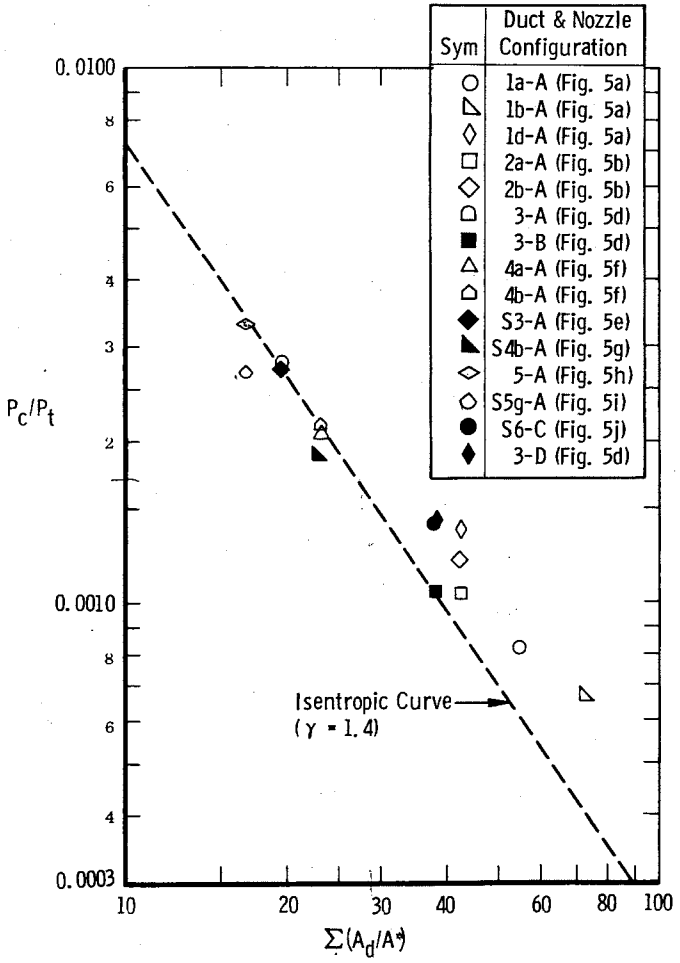

Fig. 18 Diffuser Cell-to-Driving Pressure Ratio Compared to One-Dimensional Isentropic Pressure Ratio

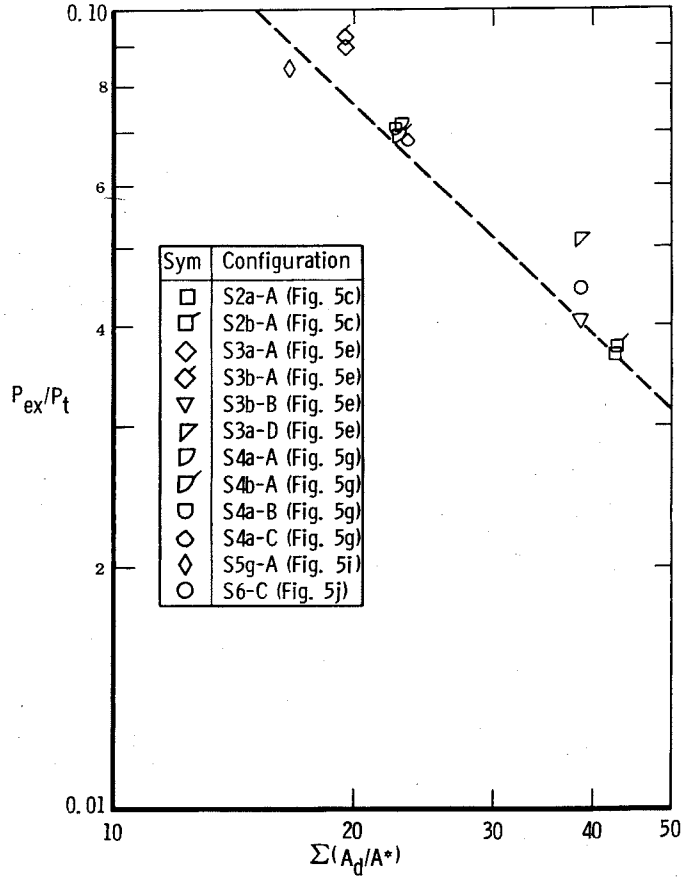

Fig. 19 Second Throat Diffuser-Ejector Driving Pressure Ratio Required for Starting

Configuration 1

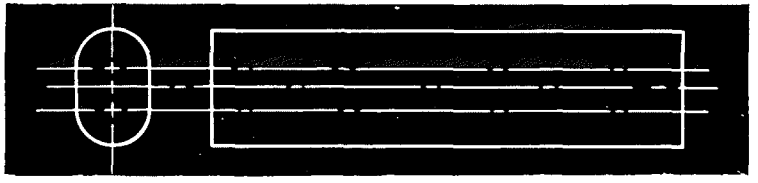

Configuration 2

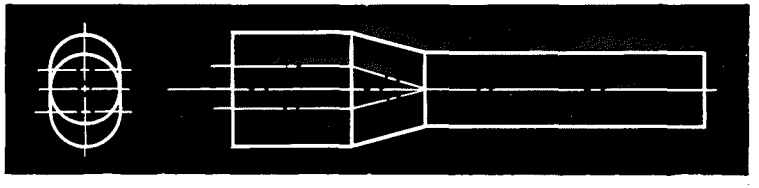

Configuration S2

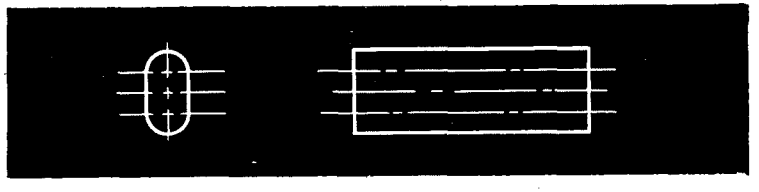

Configuration 3

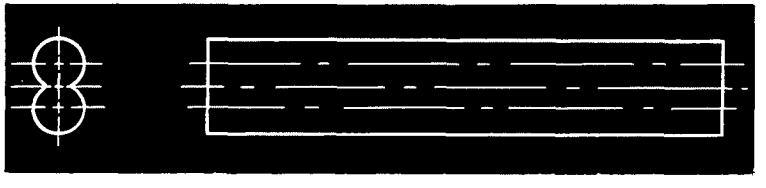

Configuration 4

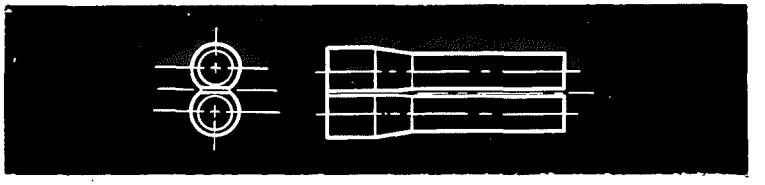

Configuration S4

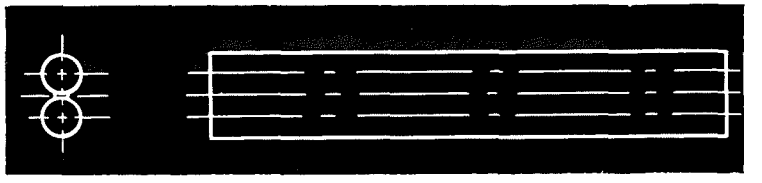

Configuration 5

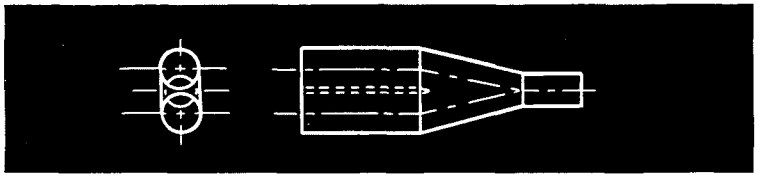

Configuration S5

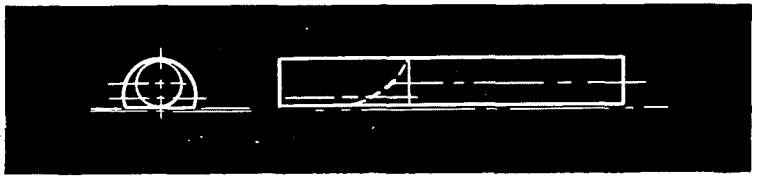

Configuration S6

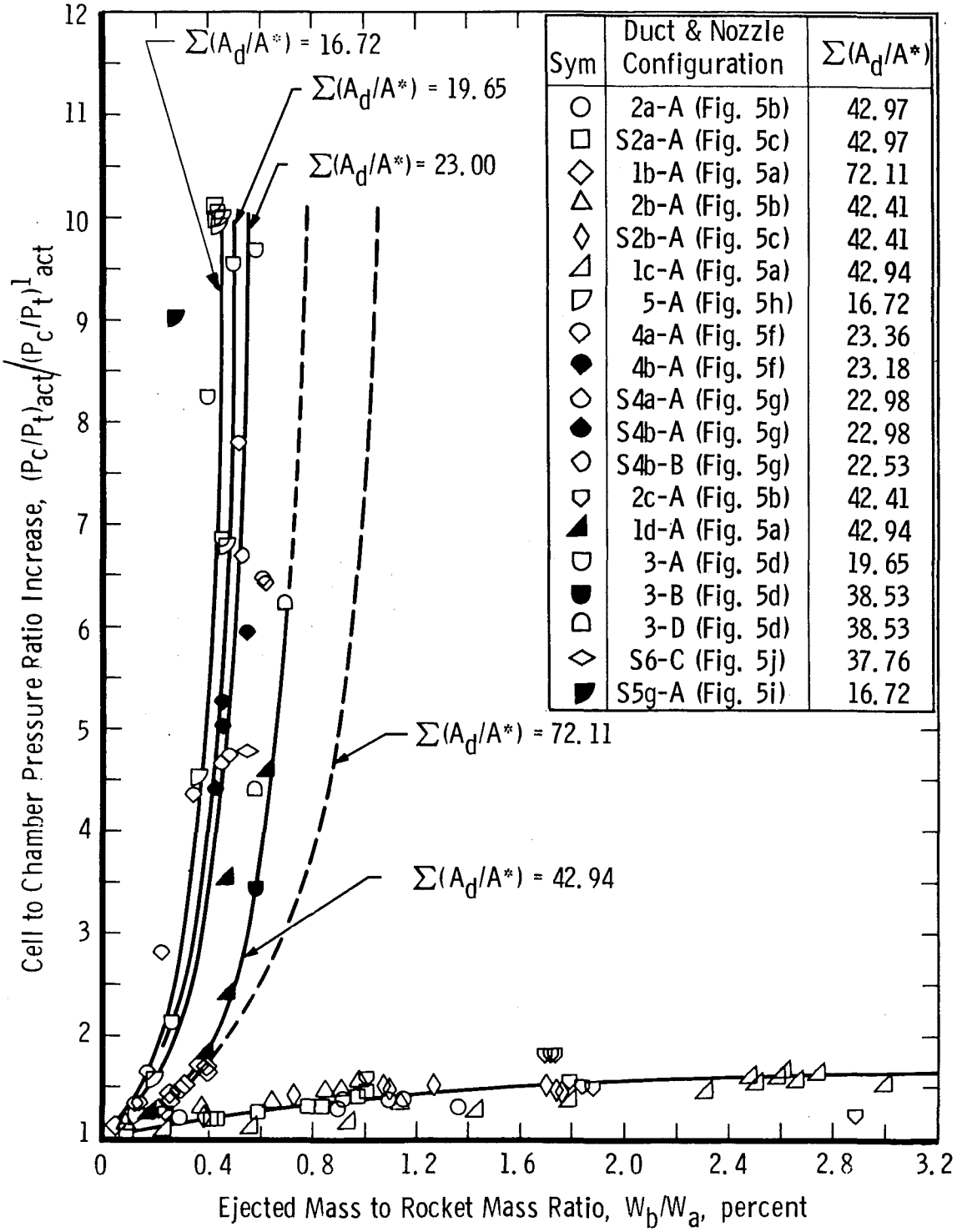

Fig. 20 Performance Improvement by Ejecting Mass from the Test Cell

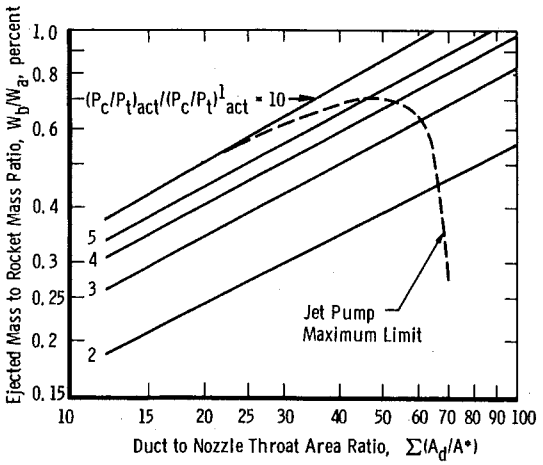

Fig. 21 Mass Ratio, W_b/W_a, Increase for Increase in Area Ratio, $\Sigma(A_d/A^*)$, at a Constant Diffuser Performance Improvement, $(P_c/P_t)_{act}/(P_c/P_t)^1_{act}$

Configuration 5

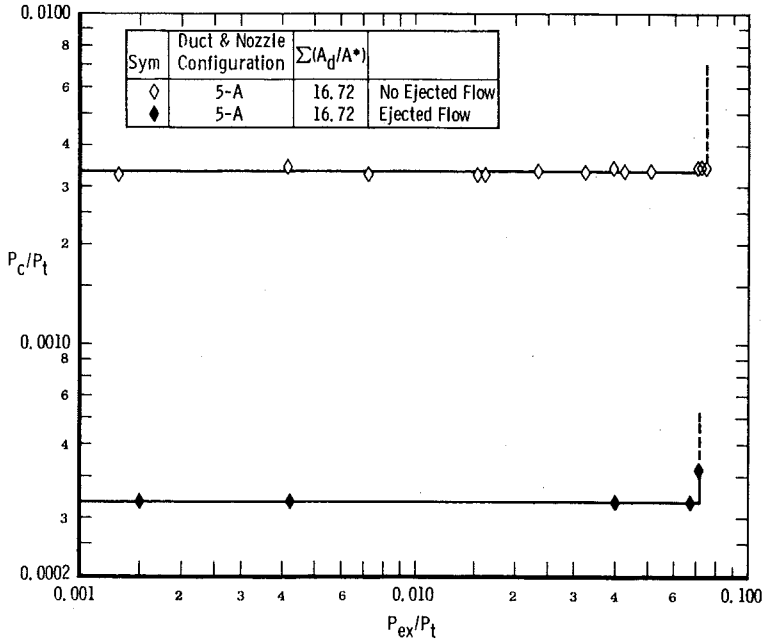

Fig. 22 Performance of Straight-Twin Circular Diffuser with and without Ejected Mass from the Test Cell